CHAPTER 5

RESULTS AND DISCUSSION
DRY SLIDING FRICTION AND WEAR BEHAVIORS

The dry sliding friction and wear behavior of CC, binary and tertiary reinforced copper hybrid composites i.e. HC-1, HC-2, HC-3, HC-4, HC-5, HC-6, HC-7 and HC-8 have been studied using the standard pin-on-disc machine under variable normal load and constant sliding speed. Hardened steel EN31 is used as counterface for the test. The prime motive for this investigation is to understand the role of ceramic reinforcements on the overall dry sliding friction and wear behaviors of both binary and tertiary reinforced copper hybrid composites. This chapter presents the results of this investigation followed by the discussion in the context of existing information from open literature as reported in Chapter-2.

5.1. Dry sliding friction and wear

Dry sliding friction and wear tests have been executed by sliding a cylindrical pin with a flat polished surface against EN 31 hardened steel disc counter face under ambient conditions using a pin-on-disc machine considering the procedures as described in Chapter-3. The sliding friction and wear tests have been executed at four different normal loads of 9.81, 19.62, 29.43, and 39.24 N and a constant sliding speed of 2.43 $m.s^{-1}$ for both binary and tertiary reinforced hybrid composites. The relative humidity has been kept in the range between 50-80% during the conduct of dry sliding friction and wear tests. The cumulative weight loss with increasing sliding distance has been measured and converted into cumulative volume loss by dividing with the density of the respective test specimen. Three repeated tests have been performed and the average cumulative volume loss (V) as a function of sliding

distance (*S*) has been reported as the basic result under dry sliding condition. The wear rate (*V/S*), in units of mm^3/m, for a given specimen under a given condition of sliding, has been evaluated from the slope of the linear variation of cumulative volume loss with sliding distance as estimated by the linear least square fit. However, the coefficient of friction is calculated by dividing the frictional force by applied normal force.

5.2. Dry sliding friction and wear of binary reinforced copper-based hybrid composites

5.2.1. Dry sliding friction

5.2.1.1. Variation of coefficient of friction with sliding distance

Figures 5.1 (a) to (d) display the behavior of the coefficient of friction with sliding distance of CC, HC-1, HC-2, HC-3 and HC-4 at constant normal loads of 9.81, 19.62, 29.43, 39.24 N and sliding speed of 2.43 $m.s^{-1}$. The behavior of friction coefficient with sliding distance is fluctuating in nature. From the Fig 5.1, it is also observed that at low loads such as 9.81 and 19.62 N the friction coefficient range varies from 0.4 to 0.97 and 0.65 to 0.99, respectively. However, in case of higher loads, the fluctuating range of friction coefficient lies in between 0.55 to 0.9. The least friction coefficient is observed for CC and most for HC-4. Overall, CC shows lower friction coefficient than hybrid composite materials.

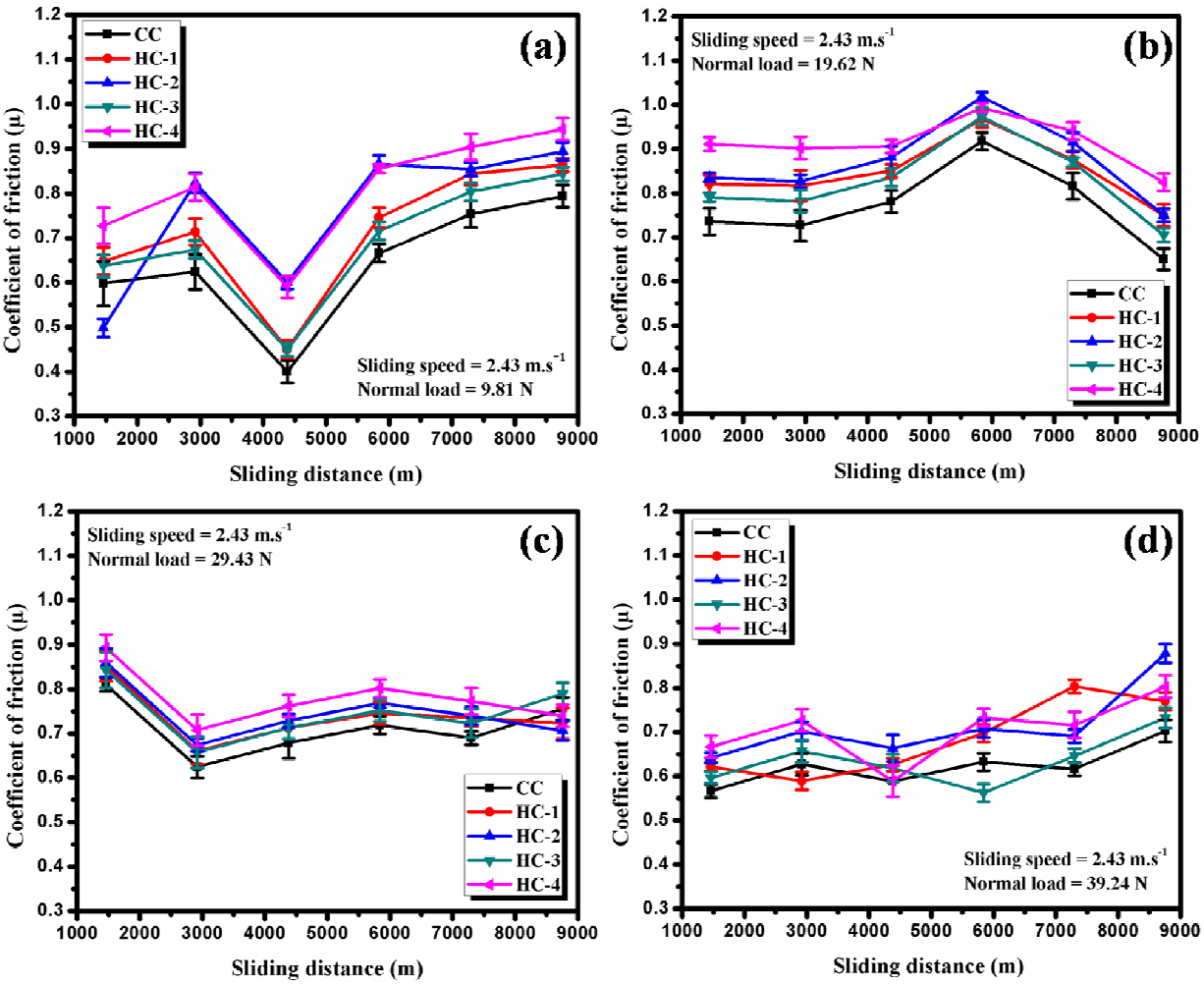

Fig.5.1. Variation of coefficient of friction with sliding distance at normal load of (a) 9.81 N, (b) 19.62 N, (c) 29.43 N and (d) 39.24 N at a constant speed of 2.43 $m.s^{-1}$

5.2.1.2. Variation of average coefficient of friction with normal load

Figure 5.2 shows the variation of average coefficient of friction with normal load of CC, HC-1, HC-2, HC-3 and HC-4 for sliding distance of 8,748 m at constant sliding speed of 2.43 $m.s^{-1}$. From the Fig. 5.2, it is found that the average friction coefficient of CC is lower compared with all hybrid composites at all the normal loads. The highest average coefficient of friction is found in HC-4 at all the loads. It is also observed that the average coefficient of friction of all the materials investigated simply decreases as the applied normal load

increases. However, the Fig. 5.2 indicates that the average friction coefficient increases up to normal load of 19.62 N for all the materials tested and further it decreases up to the normal load of 39.24 N.

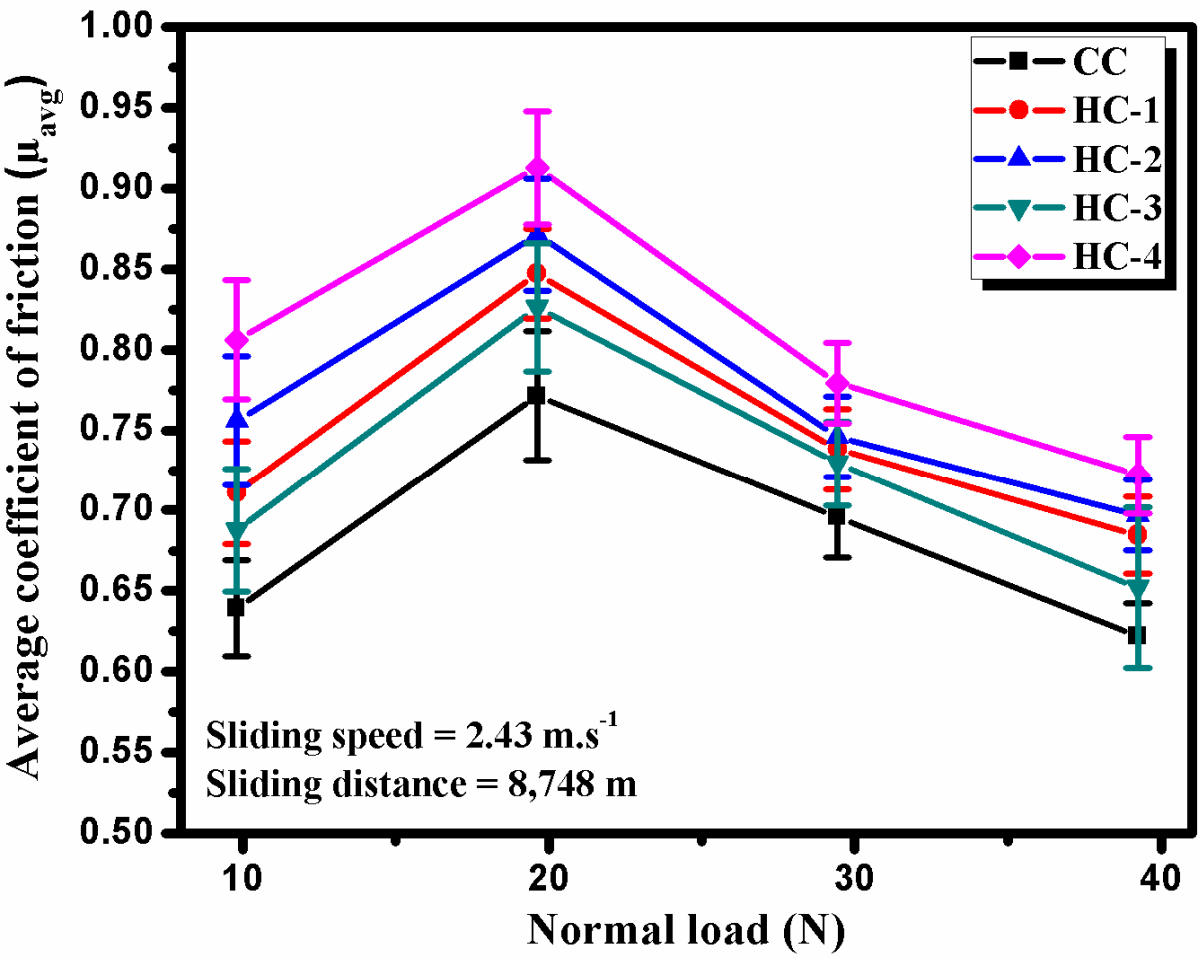

Fig.5.2. Variation of average coefficient of friction with normal load at a constant sliding speed of 2.43 m.s^{-1} and constant sliding distance of 8,748 m

5.2.1.3. Variation of average coefficient of friction with hardness

The behavior of average friction coefficient with hardness, at normal loads of 9.81, 19.62, 29.43 and 39.24 N for CC, HC-1, HC-2, HC-3 and HC-4 at a constant sliding speed of 2.43 m.s^{-1} for sliding distance of 8,748 m is depicted in Fig. 5.3. From the Fig. 5.3 it can be

observed that at all the normal loads, average coefficient of friction increases with increasing hardness of the materials. It is also observed that the average coefficient of friction has highest increasing propensity with increasing hardness at normal load of 19.62 N and it has the lowest increasing tendency at normal load of 39.24 N.

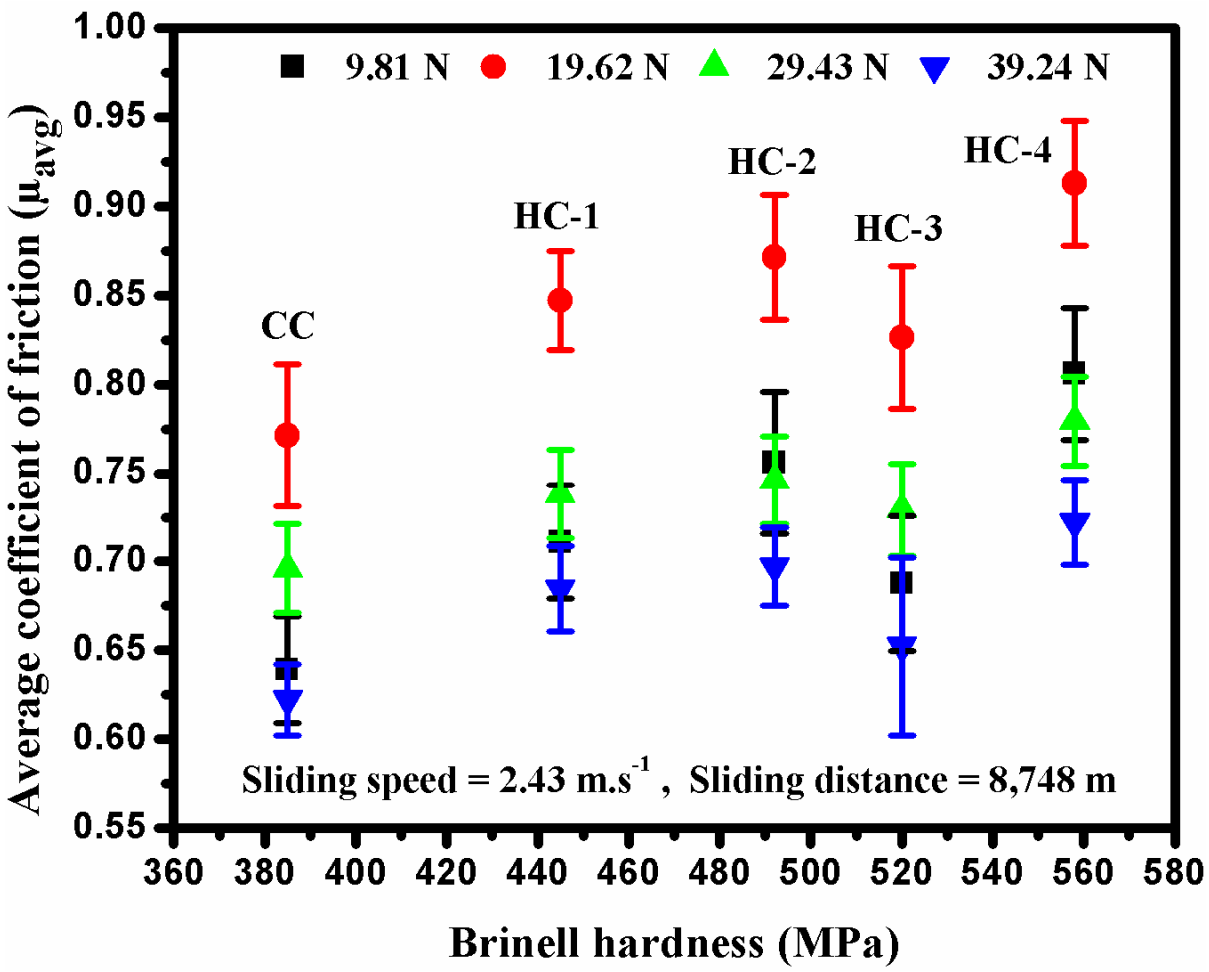

Fig.5.3. The variation of the average coefficient of friction with hardness under 9.81, 19.62, 29.43 and 39.24 N for CC, HC-1, HC-2, HC-3 and HC-4 at a constant sliding speed of 2.43 $m.s^{-1}$ and sliding distance of 8,748 m.

5.2.2. Dry sliding wear

5.2.2.1. Variation of cumulative volume loss with sliding distance

The cumulative volume loss with sliding distance of CC, HC-1, HC-2, HC-3 and HC-4 are shown in Figs. 5.4 (a) to (d) under normal loads of 9.81, 19.62, 29.43 and 39.24 N and at a constant sliding speed of 2.43 $m.s^{-1}$. The calculated values of weight loss for the entire sample tested were converted into volume loss by dividing the density of the respective sample. The sliding distance covered during the wear test was 8,748 m total. At all normal loads cumulative volume loss increases linearly with increasing sliding distance. The cumulative volume loss of CC, HC-1, HC-2, HC-3 and HC-4 is found to be 7.55, 5.49, 4.39, 5.22 and 3.11 mm^3 at 9.81N load, respectively. The volume loss at 19.62 N load is found to be 9.73, 6.05, 4.88, 5.86, 4.26 mm^3. The volume loss at load 29.43 N is 9.50, 6.60, 5.44, 6.22 and 4.73 mm^3 whereas at 39.24 N is 8.55, 6.99, 5.69, 6.68 and 5.12 mm^3, respectively. The cumulative volume loss shown by CC is the largest among all the materials investigated at all normal loads whereas the cumulative volume loss shown by the HC-4 is the smallest as shown in Figs. 5.4 (a) to (d), respectively. It can also be seen that the cumulative volume loss for HC-3 is higher compared with HC-2 at all normal loads. In comparison to HC-4 it is found that the volume loss for CC is 58.82, 56.22, 50.21 and 40.12% higher at the various loads of 9.81, 19.62, 29.43 and 39.24 N, respectively.

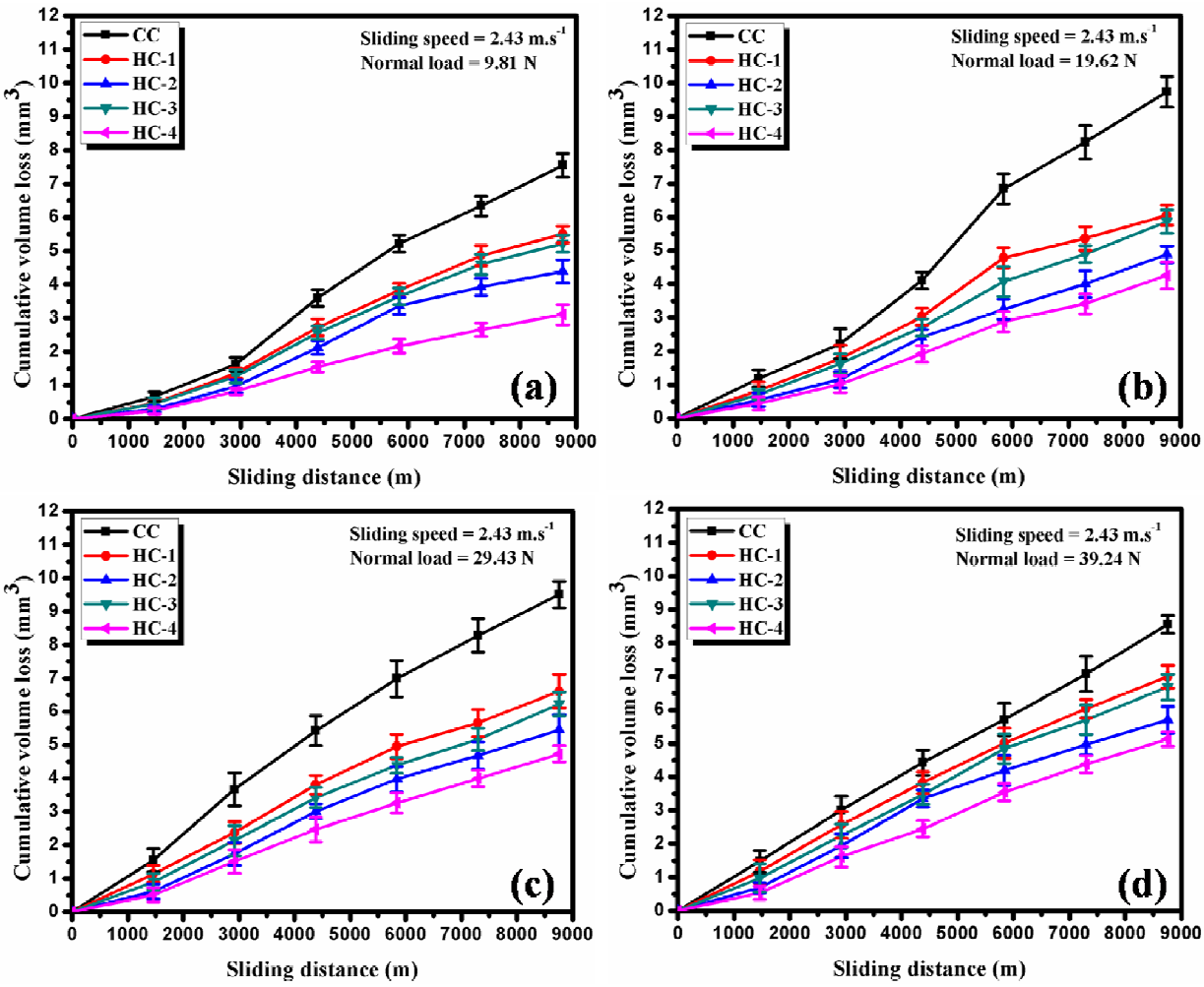

Fig.5.4. Variation of cumulative volume loss with sliding distance at normal load of (a) 9.81 N, (b) 19.62 N, (c) 29.43 N and (d) 39.24 N for a constant sliding speed of 2.43 $m.s^{-1}$

5.2.2.2. Variation of wear rate with normal load

Figure 5.5 displays the trend of wear rate with normal load of CC, HC-1, HC-2, HC-3 and HC-4 at constant sliding speed of 2.43 $m.s^{-1}$ and sliding distance of 8,748 m. The rate of wear at a given load has been estimated from the gradient of the variation of cumulative volume loss with sliding distance presented in Fig. 5.4 for all the materials investigated. From the Fig. 5.5, it can be observed that the rate of wear increases almost linearly for entire materials used in the current investigation. However, the wear rate shown by CC is the

highest and HC-4 has the lowest wear rate among entire materials at all the normal loads. Whereas the rates of wear shown by other hybrid composites in the same band at all normal loads but it increases with increasing load, as can be observed in Fig. 5.5. The wear rate variation with normal load of HC-3 lies in between the variation of HC-1 and HC-2 at all the loads with similar pattern as shown in Fig. 5.5.

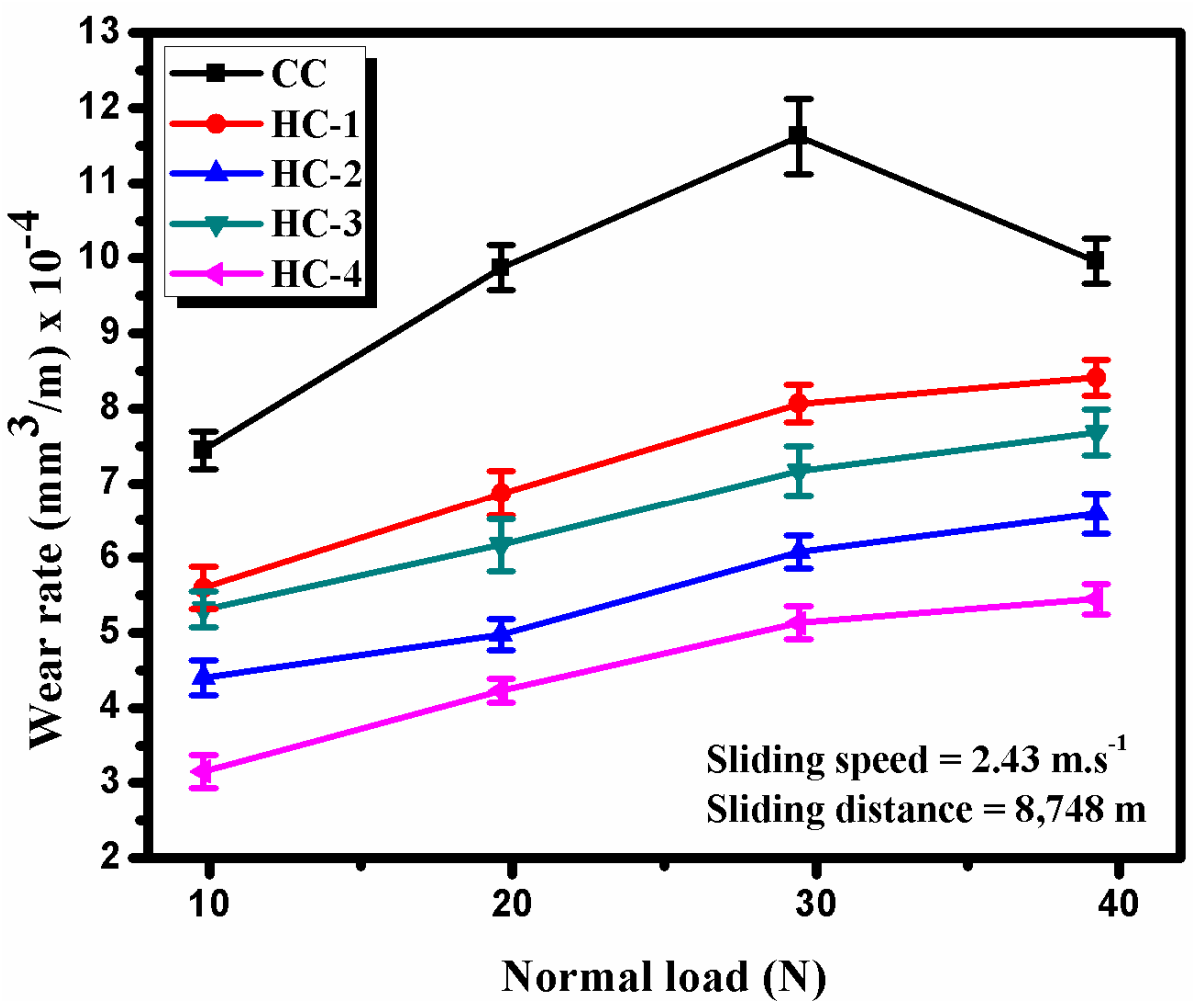

Fig.5.5. Variation of wear rate with normal load at a constant sliding speed of 2.43 $m.s^{-1}$ and sliding distance of 8,748 m

5.2.2.3. Variation of wear rate with hardness

Figure 5.6 displays the variation of wear rate with hardness under lowest loads of 9.81 N and highest load of 39.24 N for CC, HC-1, HC-2, HC-3 and HC-4 at constant sliding speed of 2.43 $m.s^{-1}$ and sliding distance of 8,748 m. It can be observed from the Fig.5.6 that the rate of wear decreases with increasing hardness of the materials for both the load of 9.81 and 39.24 N. The similar trend is also observed for normal load of 19.62 and 29.43 N which is not reported here. It can be seen from the Fig. 5.6, the rate of wear with hardness under low normal load 9.81 is lower as compared with under high load of 39.24 N.

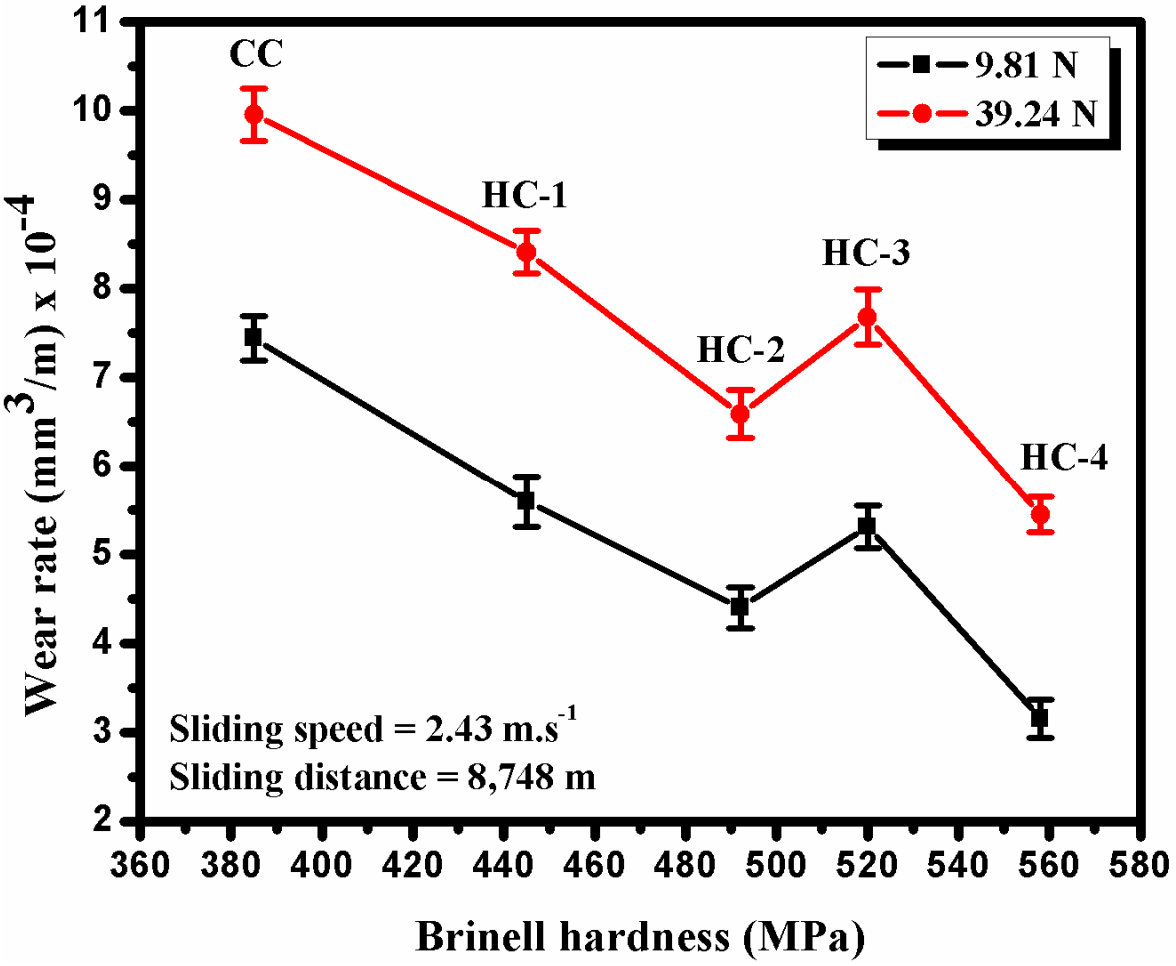

Fig.5.6. Variation of wear rate with Brinell hardness at a constant sliding speed of 2.43 $m.s^{-1}$ and sliding distance of 8,748 m

5.2.3. Examination of worn surfaces

5.2.3.1. Worn surfaces at normal load of 9.81 N

Figures 5.7 (a) to (e) show the SEM micrographs of the worn surfaces of CC, HC-1, HC-2, HC-3 and HC-4, respectively, after sliding distance of 8,748 m at a normal load of 9.81 N and a constant sliding speed of 2.43 $m.s^{-1}$. Some grooves running along the direction of sliding along with a transfer layer of wear debris could be observed on all the worn surfaces of hybrid materials investigated. However, the grooves appear to be deeper in case of CC in comparison to those observed on the worn surface of hybrid composites as evident from Figs. 5.7 (a) and (e). Delamination is also observed on the worn surface of CC and it is higher compared with other worn surfaces. Almost no grooves could be observed on the worn surface of HC-4 which appears to be completely covered by the transfer layer as depicted in Fig. 5.7 (e). The extent of transfer layer appears to be more on the worn surface of HC-4 as compared with HC-3.

5.2.3.2. Worn surfaces at normal load of 39.24 N

SEM micrograph of the worn surface of CC, HC-1, HC-2, HC-3 and HC-4 are shown in Figs. 5.8 (a) to (e) respectively at constant normal load of 39.24 N and sliding speed of 2.43 $m.s^{-1}$ for the sliding distance of 8,748 m. Morphology of the worn surface of the hybrid composites is notably dissimilar than the worn surface of CC. Severe plastic deformation, delamination, scratch and quite oxidative layers are observed in the worn surfaces of CC as shown in Fig. 5.8 (a). However, quite delamination, narrow grooves, transfer layers and wear debris are observed on the worn surfaces of all hybrid composites as shown in Figs. 5.8 (b) to (e). The worn surfaces of HC-1 and HC-3 also show the cracks and mechanically mixed layer

(MML) as shown in Figs. 5.8 (b) and (d). Among all the worn surfaces of materials, HC-4 shows the least irregularity on its worn surfaces which indicates its least wear among all.

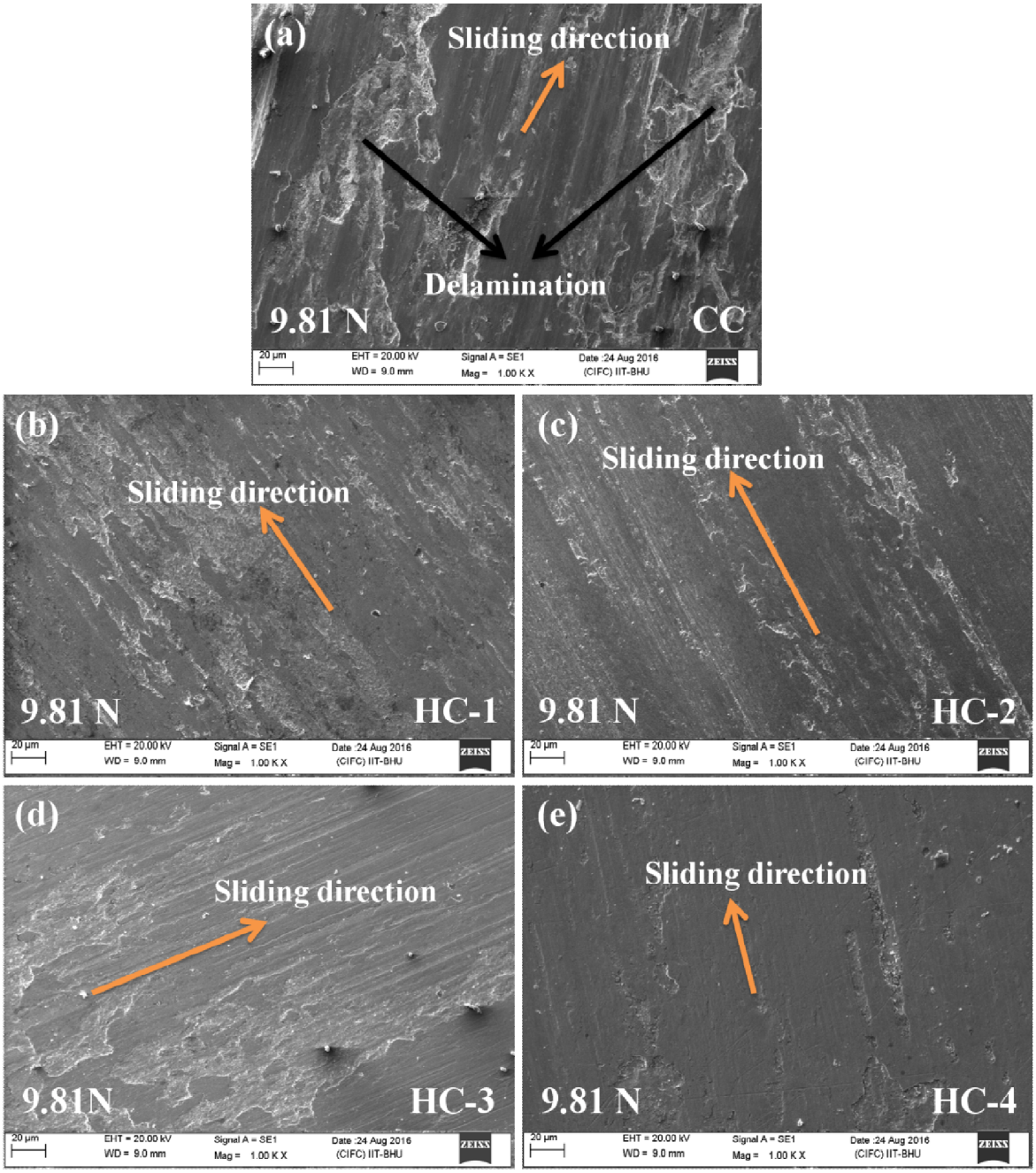

Fig.5.7. SEM micrographs of worn surface of (a) CC, (b) HC-1, (c) HC-2, (d) HC-3 and (e) HC- 4 at load of 9.81 N and sliding speed of 2.43 $m.s^{-1}$ for sliding distance of 8,748 m

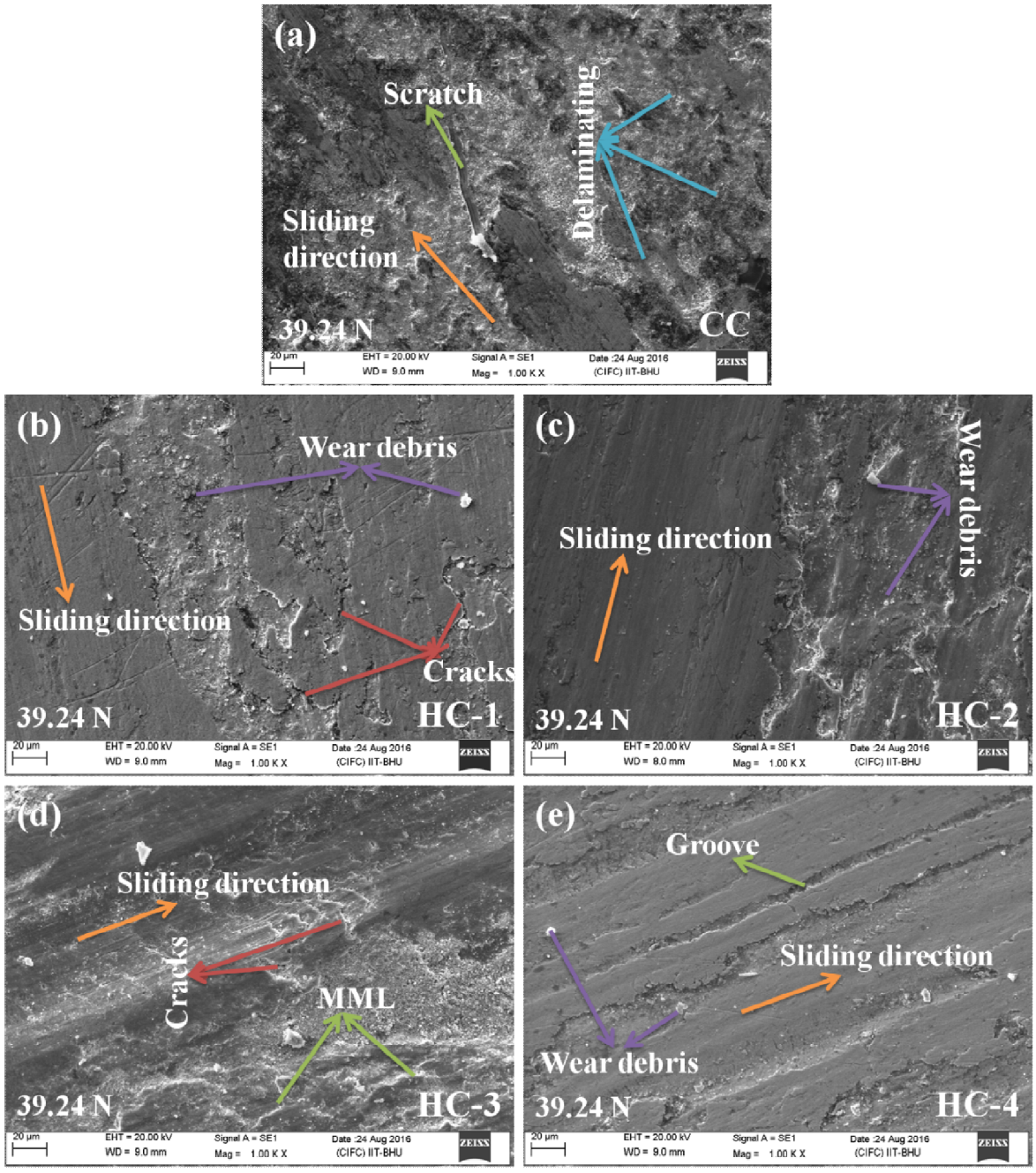

Fig.5.8. SEM micrographs of worn surface of (a) CC, (b) HC-1, (c) HC-2, (d) HC-3 and (e) HC-4 at load of 39.24 N and sliding speed of 2.43 $m.s^{-1}$ for sliding distance of 8,748 m

5.2.3.3. EDAX spectrum of worn surfaces at 39.24 N

Figures 5.9 (a) to (e) show the EDAX spectrum of the worn surface of the CC, HC-1, HC-2, HC-3 and HC-4, respectively at constant sliding speed of 2.43 $m.s^{-1}$ and normal load of 39.42 N for the sliding distance of 8,748 m. This investigation is conducted on worn surfaces of the materials to understand the wear mechanisms which govern the tribological behaviors of CC, HC-1, HC-2, HC-3 and HC-4 during dry sliding. It is observed that the presence of small intensity peak of the oxygen in the entire EDAX spectrum, its weight and atomic percentage are given in the table just by side their spectrums. It indicates that the some oxide layer has been developed on the worn surfaces of developed materials during the dry sliding. From the Fig. 5.9, it can be see the intensity peaks of almost all the reinforcing elements present in the EDAX spectrum of respective materials. However, in the EDAX spectrum of the HC-3, the intensity peaks of carbon and tungsten are not observed as show in Fig. 5.9 (d). A new intensity peak of iron which does not belong to the reinforcing family is observed in EDAX spectrum of the HC-1, HC-2, HC-3 and HC-4 as shown in Figs. 5.9 (b) to (e), respectively.

5.2.4. Examination of wear debris

Figures 5.10 (a) to (e) show the SEM morphology of the wear debris of CC, HC-1, HC-2, HC-3 and HC-4, respectively at sliding speed of 2.43 $m.s^{-1}$ and normal load of 39.24 N after sliding over the distance of 8,748 m. The morphology of the wear debris is studied at same scale of 5000 X. The larger, plate like and flaky geometry of the wear debris of CC are observed as shown in Fig. 5.10 (a). From the Fig. 5.10, it is observed that the size of wear debris of hybrid composites is comparatively lower than the wear debris of CC. The

morphology of the wear debris of hybrid composites display almost zero flaky and plate like debris particles as shown in Figs. 5.10 (b) to (e). Some agglomerated debris particles can be observed in the morphology of wear debris of HC-1, HC-2 and HC-3 as shown in Figs. 5.10 (b) to (d) respectively.

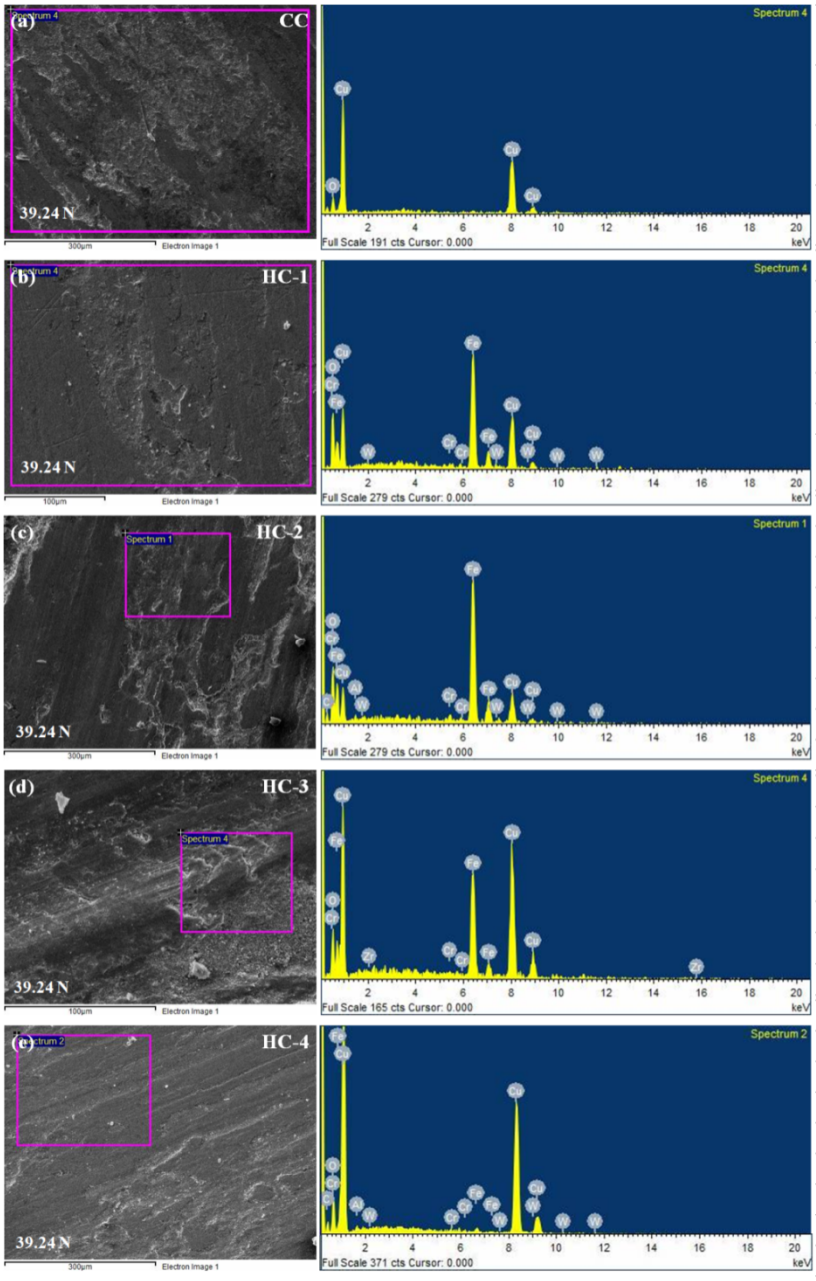

Element	Weight%	Atomic%
O K	10.67	32.18
Cu K	89.33	67.82
Totals	100.00	

Element	Weight%	Atomic%
O K	16.45	42.25
Cr K	0.34	0.27
Fe K	42.18	31.04
Cu K	40.80	26.39
W M	0.24	0.05
Totals	100.00	

Element	Weight%	Atomic%
C K	19.81	43.81
O K	15.83	26.29
Al K	0.59	0.59
Cr K	0.96	0.49
Fe K	46.40	22.07
Cu K	16.00	6.69
W M	0.40	0.06
Totals	100.00	

Element	Weight%	Atomic%
O K	10.67	31.32
Cr K	0.34	0.31
Fe K	25.72	21.63
Cu K	63.13	46.67
Zr L	0.15	0.08
Totals	100.00	

Element	Weight%	Atomic%
C K	17.70	45.81
O K	9.42	18.30
Al K	0.47	0.54
Cr K	0.01	0.01
Fe K	0.90	0.50
Cu K	71.07	34.76
W M	0.43	0.07
Totals	100.00	

Fig.5.9. EDAX spectrum of worn surface of (a) CC, (b) HC-1, (c) HC-2, (d) HC-3 and (e) HC-4 at load of 39.24 N and sliding speed of 2.43 $m.s^{-1}$ for sliding distance of 8,748 m

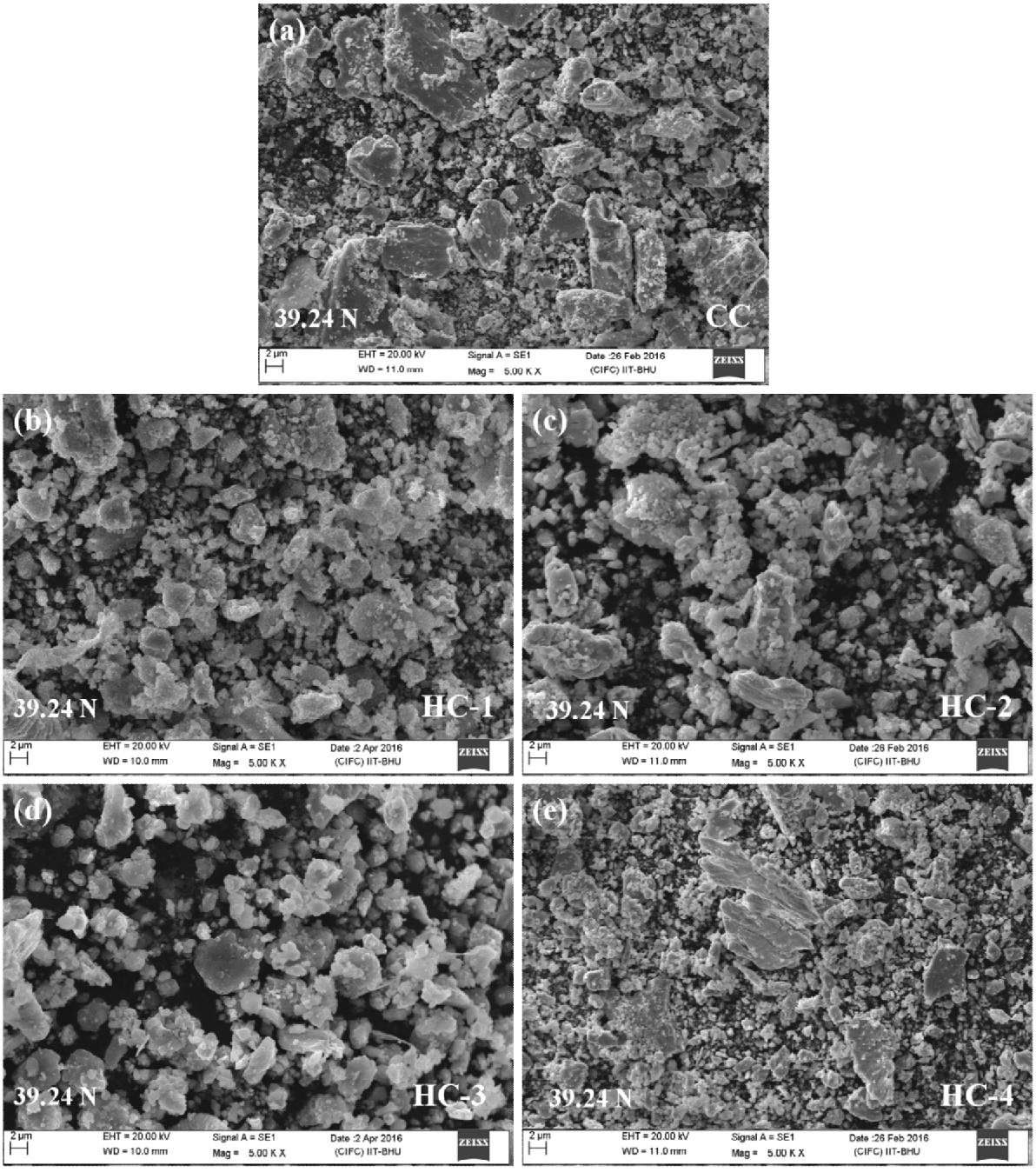

Fig.5.10. SEM morphology of wear debris of (a) CC, (b) HC-1, (c) HC-2, (d) HC-3 and (e) HC-4 at load of 39.24 N and sliding speed of 2.43 $m.s^{-1}$ for sliding distance of 8,748 m

5.2.5. AFM analysis of worn surfaces

The atomic force microscopic (AFM) morphology of the worn surfaces of CC, HC-1, HC-2, HC-3 and HC-4 are depicted in Figs. 5.11 (a) to (e) respectively at sliding speed of 2.43 $m.s^{-1}$ and normal load of 39.24 N over the sliding distance of 8,748 m. Basically, this characterization is done on worn surfaces of the materials for quantitative analysis of its roughness in terms of root-mean-square deviation of profile (R_q) and arithmetical mean deviation of profile (R_a). From the Figs. 5.11 (a) to (e), it is clearly observed that the R_a (0.225 µm) and R_q (0.238 µm) value of worn surface of CC is much higher than the R_a and R_q value of worn surfaces of hybrid composites. Among all the worn surfaces of materials, HC-4 exhibits the least value of R_a (0.024 µm) and R_q (0.031 µm).

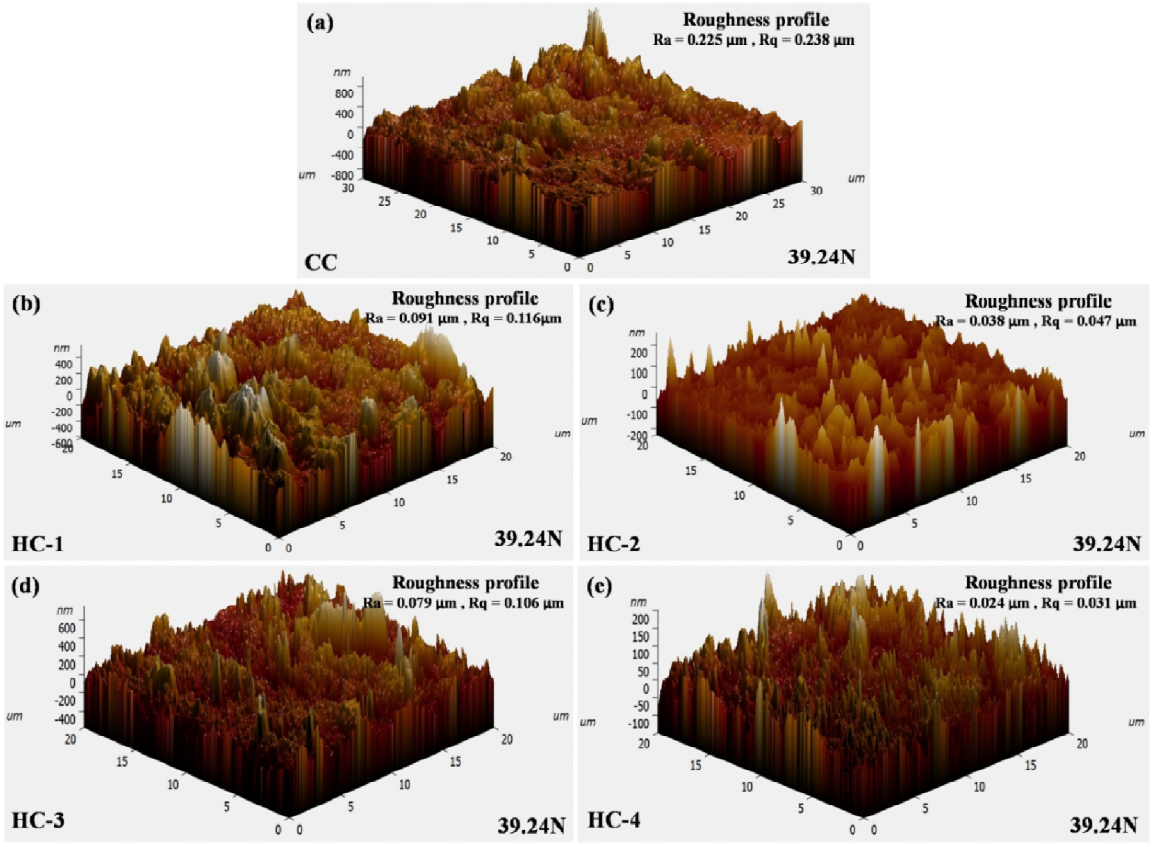

Fig.5.11. AFM morphology of worn surface of (a) CC, (b) HC-1, (c) HC-2, (d) HC-3 and (e) HC-4 at load of 39.24 N and sliding speed of 2.43 $m.s^{-1}$ for sliding distance of 8,748 m

5.3. Dry sliding friction and wear of tertiary reinforced copper-based hybrid composites

5.3.1. Dry sliding friction

5.3.1.1. Variation of coefficient of friction with sliding distance

The typical variation of friction coefficient with sliding distance at normal load of 9.81, 19.62, 29.43 and 39.24 N for CC, HC-5, HC-6, HC-7 and HC-8 hybrid composites at a constant sliding speed of 2.43 $m.s^{-1}$ against the EN31 hardened steel counter face have been shown in Figs.5.12 (a) to (d). The friction coefficient is observed to fluctuate and the amplitude of fluctuations is observed to decrease with increasing distance of sliding at variable normal loads for entire materials studied in the current investigation as evident from Figs. 5.12 (a) to (d). The range of coefficient of friction at 9.81 N load is 0.4 - 0.79, at 19.62 N load is 0.48 - 0.92, at 29.43 N load is 0.52- 0.81 and at 39.24 N load it is 0.49 - 0.7.

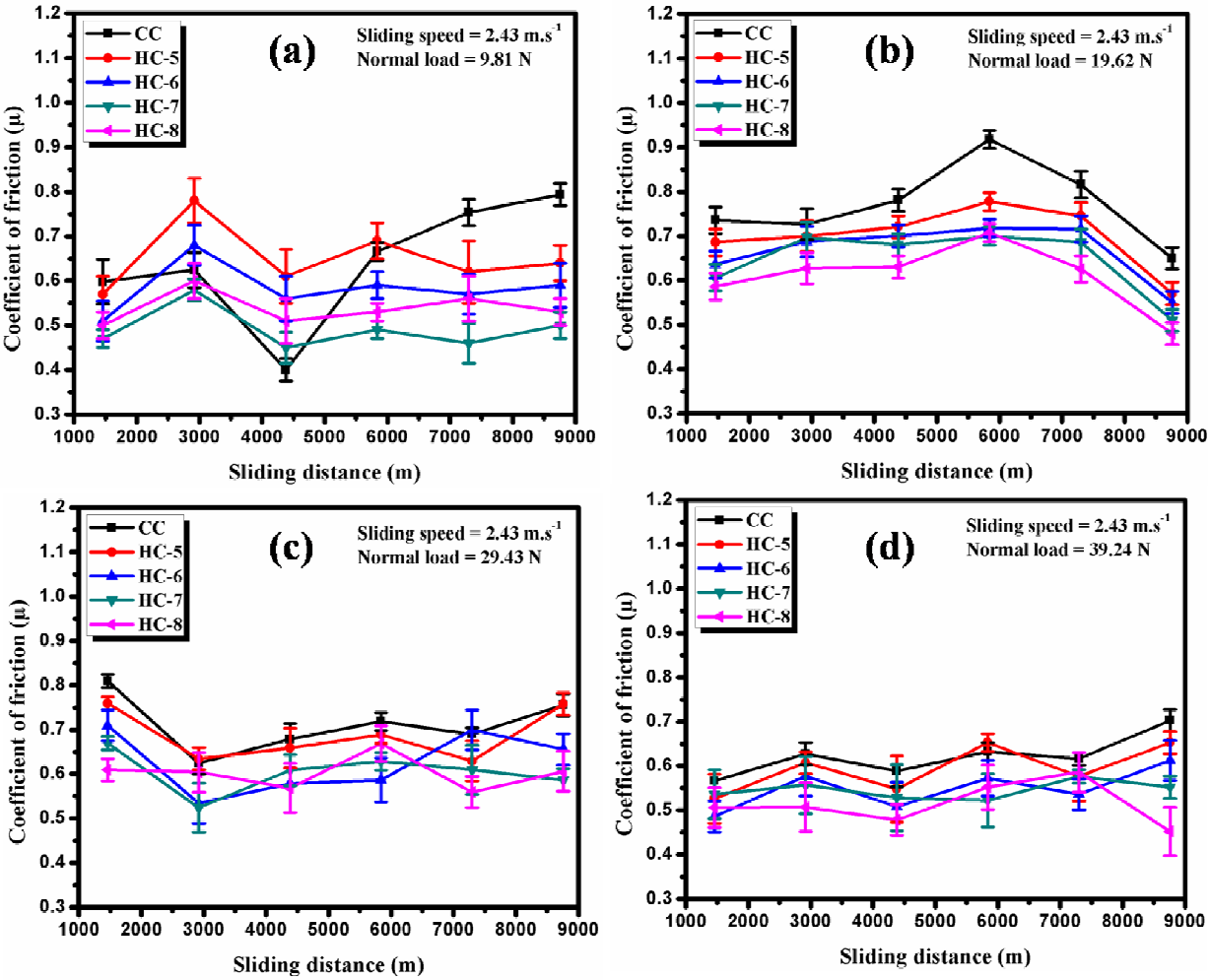

Fig.5.12. Variation of coefficient of friction with sliding distance at normal load of (a) 9.81 N, (b) 19.62 N, (c) 29.43 N and (d) 39.24 N at a constant speed of 2.43 $m.s^{-1}$

5.3.1.2. Variation of average coefficient of friction with normal load

The average friction coefficient with normal load at a constant sliding speed of 2.43 $m.s^{-1}$ for CC, HC-5, HC-6, HC-7 and HC-8 hybrid composites over the sliding distance of 8,748 m are shown in Fig. 5.13. It is observed that the average friction coefficient of decreases with increasing normal load for all the materials investigated. However, the average friction coefficient initially increases as the load increases from 9.81 to 19.62 N for all the materials investigated and then decreases as the load is increased to 29.43 N ahead of

which it increases till 39.24 N normal load. It is also found that the average friction coefficients of hybrid composites are lesser compared with CC. It could also be observed from Fig. 5.13 that the average coefficient of friction revealed by all the materials lie in between 0.48 to 0.78. However, the average coefficient of friction shown by HC-8 is the lowest and CC is the highest among all at all the normal loads.

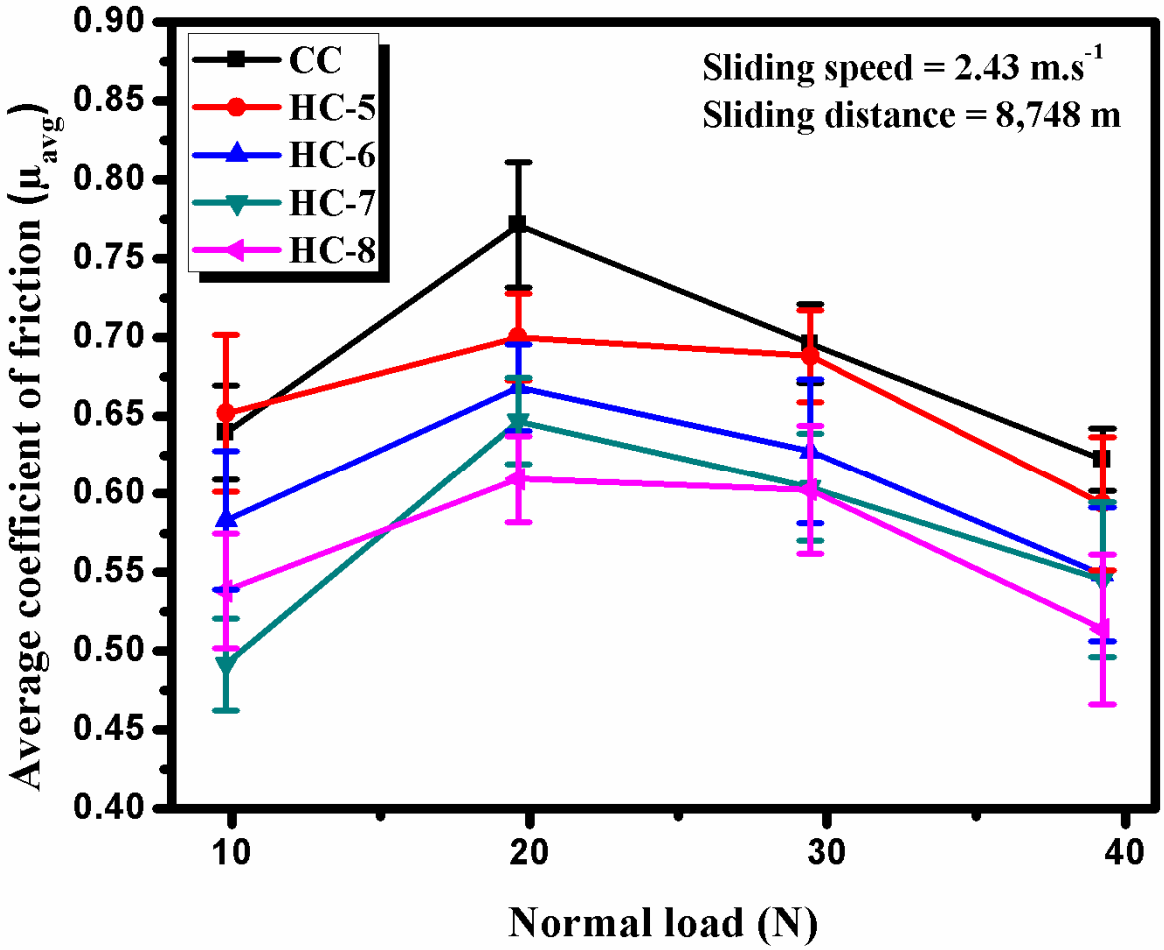

Fig.5.13. Variation of average coefficient of friction with normal load at a constant sliding speed of 2.43 $m.s^{-1}$ and constant sliding distance of 8,748 m

5.3.1.3. Variation of average coefficient of friction with hardness

The variation of the average friction coefficient with hardness under normal loads of 9.81 and 39.24 N for CC, HC-5, HC-6, HC-7 and HC-8 at a constant sliding speed of 2.43 $m.s^{-1}$ and sliding distance of 8,748 m is shown in Fig. 5.14. It can be observed from the Fig 5.14 that the average friction coefficient decreases as the hardness of the materials increases at both the lower and higher normal load condition, similar trend is also observed at 19.62 N and 29.43 N so, it is not reported here. At a particular load say at 39.24 N, the declining pattern of average friction coefficient is higher compared with decreasing trend at 9.81 N load.

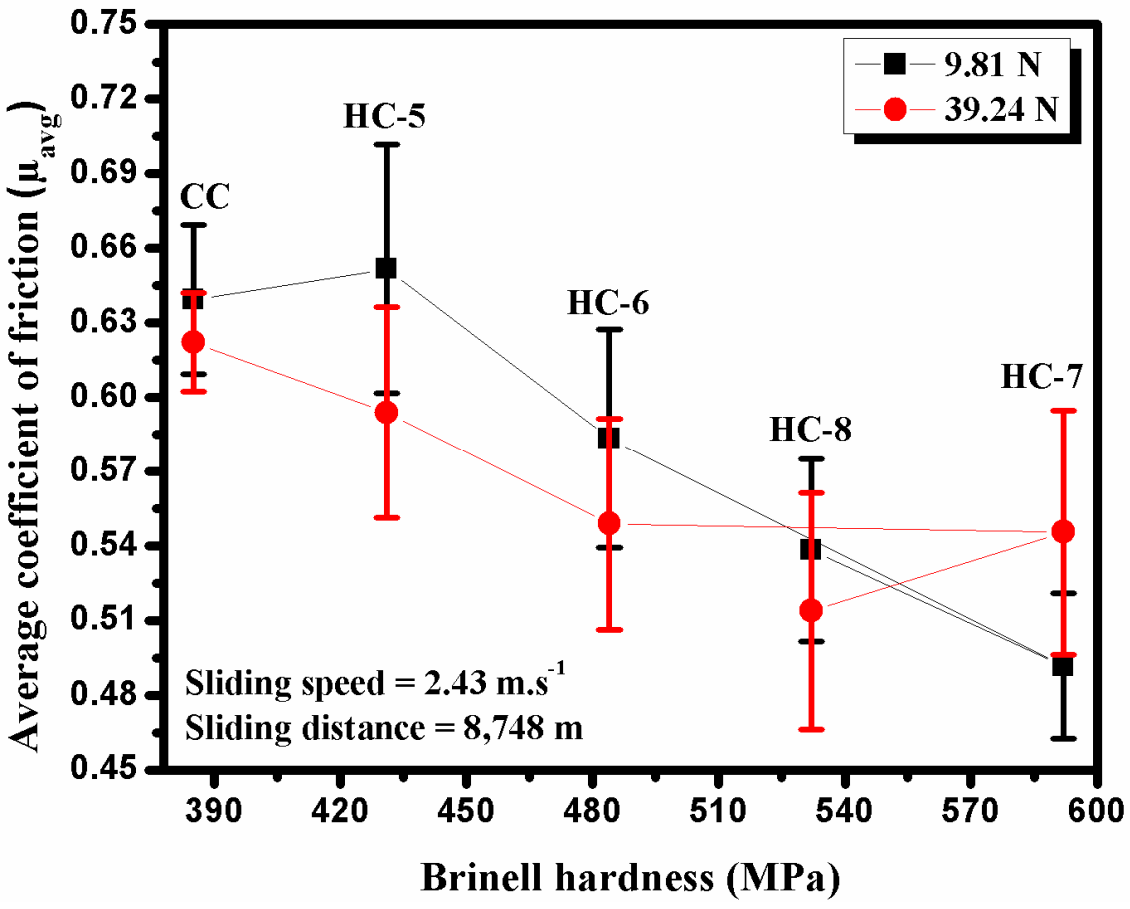

Fig.5.14. The variation of the average coefficient of friction with Brinell hardness under 9.81 N and 39.24 N for CC, HC-5, HC-6, HC-7 and HC-8 at a constant sliding speed of 2.43 $m.s^{-1}$ and sliding distance of 8,748 m

5.3.1.4. Variation of average coefficient of friction with B_4C content

Figure 5.15 illustrates the behavior of average friction coefficient with the content of B_4C at different normal loads of 9.81, 19.62, 29.43 and 39.24 N for a constant sliding speed of 2.43 $m.s^{-1}$ and sliding distance of 8,748 m. It is observed that the average coefficient of friction decreases with increase in B_4C content. However, the average coefficient of friction is found to remain almost constant as the B_4C content increase from 0.5 wt% to 1.0 wt% and 1.0 wt% to 1.5 wt% at the highest load of 39.24 N and 29.43 N respectively. B_4C reinforced hybrid composites have consistently revealed a relatively lower average coefficient of friction in comparison to the unreinforced (0 wt% of B_4C) at all the loads as seen from Fig. 5.15.

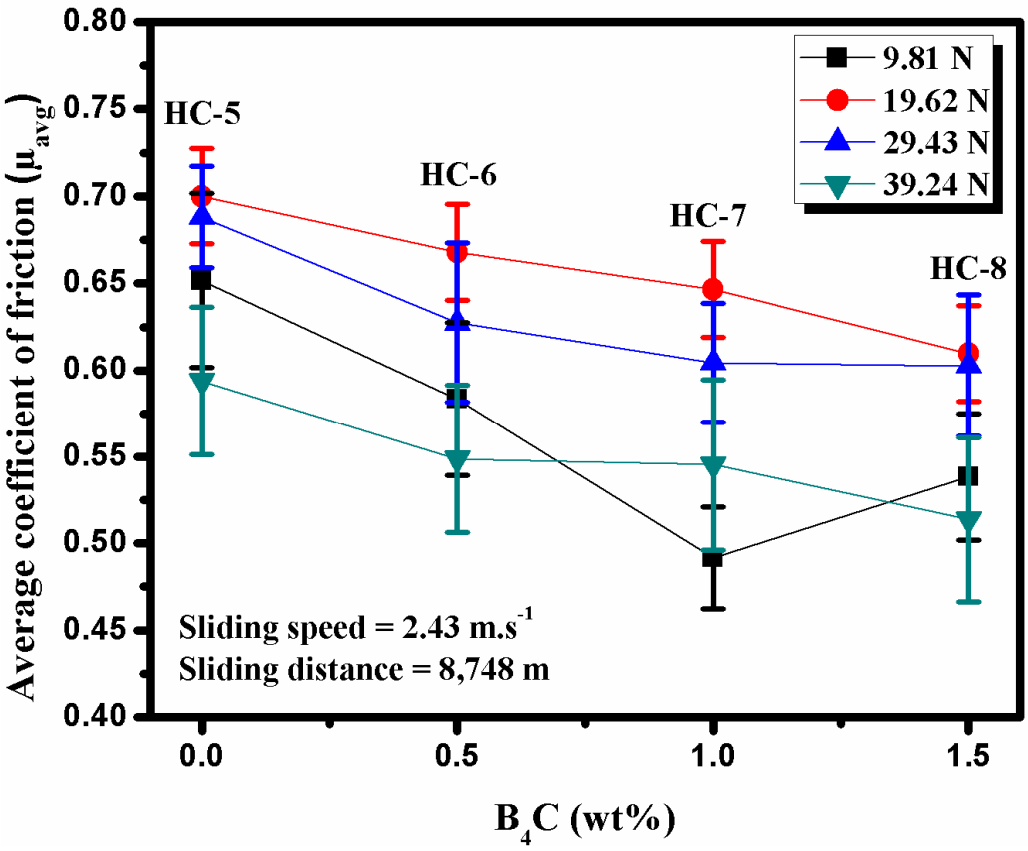

Fig.5.15. Variation of average coefficient of friction with B_4C reinforcement at normal load of 9.81, 19.62, 29.43 and 39.24 N for a constant sliding speed of 2.43 $m.s^{-1}$ and sliding distance of 8,748 m

5.3.2. Dry sliding wear

5.3.2.1. Variation of cumulative volume loss with sliding distance

Figures 5.16 (a) to (d) show the trend of cumulative volume loss with sliding distance of CC, HC-5, HC-6, HC-7 and HC-8 under different normal loads of 9.81, 19.62, 29.43 and 39.24 N at a constant sliding speed of 2.43 $m.s^{-1}$. The cumulative volume loss is evaluated by the similar way as explained in binary reinforced hybrid composites. It can be seen that the cumulative volume loss increases almost linearly with increasing sliding distance at all the normal loads. The cumulative volume loss of CC, HC-5, HC-6, HC-7 and HC-8 is found to be 7.55, 4.67, 3.50, 1.16 and 2.91 mm^3 at 9.81N load. The volume loss at 19.62 N load is found to be 9.73, 8.17, 7.0, 2.33, 4.67 mm^3. The volume loss at load 29.43 N is 9.50, 7.40, 5.98, 2.99 and 4.49 mm^3 whereas at 39.24 N is 8.55, 6.83, 5.12, 3.41and 4.27 mm^3, respectively. The cumulative volume loss observed by CC is the largest among all the materials investigated at all the normal loads whereas the cumulative volume loss shown by the HC-7 is the smallest as shown in Figs. 5.16 (a) to (d). It is also observed that the cumulative volume loss for HC-8 is higher compared with HC-7 at all normal loads. The volume loss for CC is observed to be 61.45, 52.00, 52.73 and 50.05 %, higher in comparison to HC-7 composite at the various loads of 9.81, 19.62, 29.43 and 39.24 N, respectively.

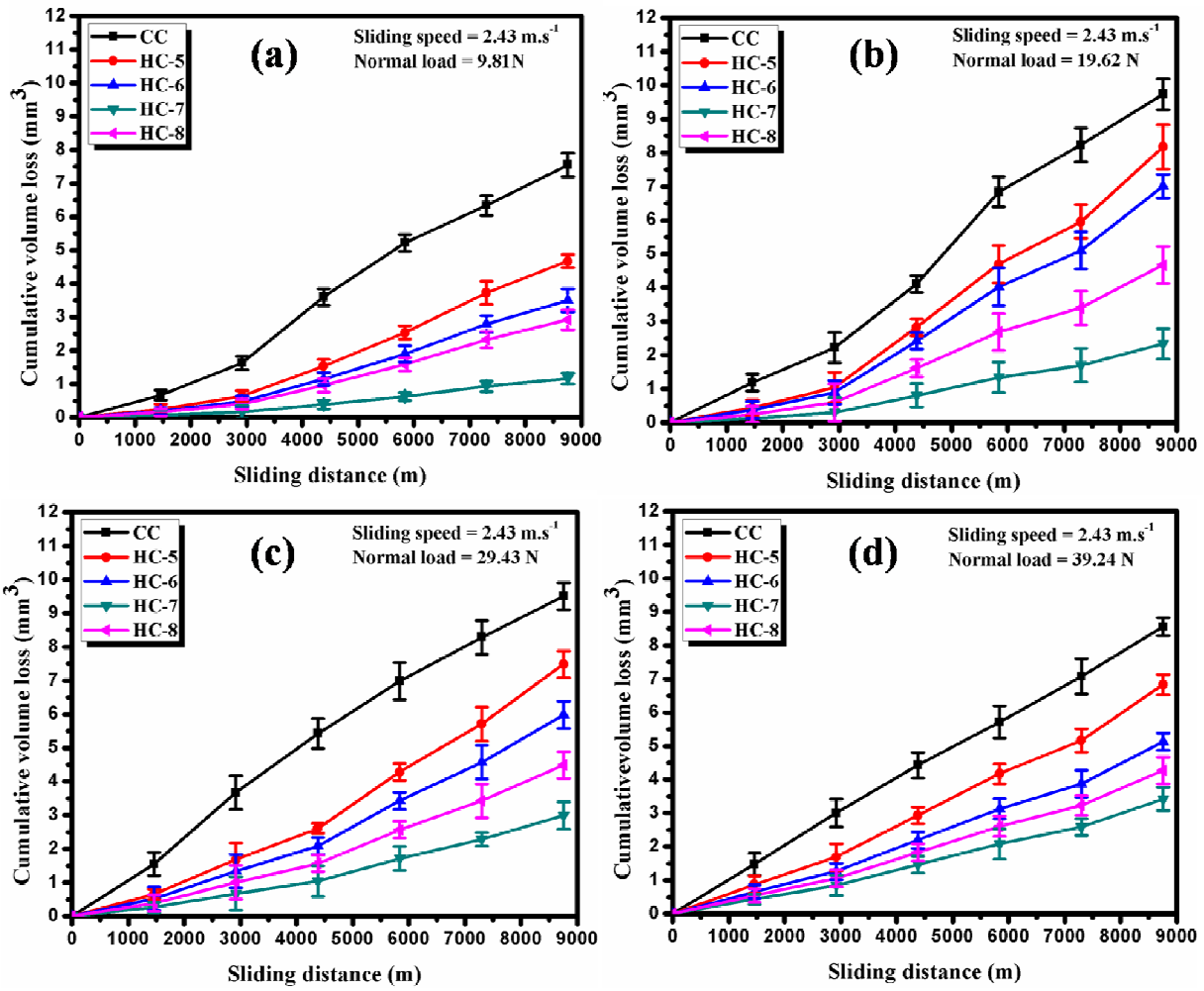

Fig.5.16. Variation of cumulative volume loss with sliding distance at normal load of (a) 9.81 N, (b) 19.62 N, (c) 29.43 N and (d) 39.24 N for a constant sliding speed of 2.43 $m.s^{-1}$

5.3.2.2. Variation of wear rate with normal load

The wear rate at a particular load has been estimated from the slope of the variation of cumulative volume loss with sliding distance presented in Fig. 5.16 for CC, HC-5, HC-6, HC-7 and HC-8, the variation of wear rate with normal load and at a constant speed of 2.43 $m.s^{-1}$ for sliding distance of 8,748 is shown in Fig. 5.17. The wear rate increases almost linearly with increasing the normal load for all the materials investigated in the present study as shown in Fig. 5.17. However, the wear rate shown by CC is higher compared with hybrid

composites at all the normal loads. Among the hybrid composites, HC-7 has shown the lowest wear rate whereas the wear rates shown by other hybrid composites are in between the wear rate of CC and HC-7. It is also observed that the wear rate of HC-8 is higher compared with HC-7 as shown in Fig. 5.17.

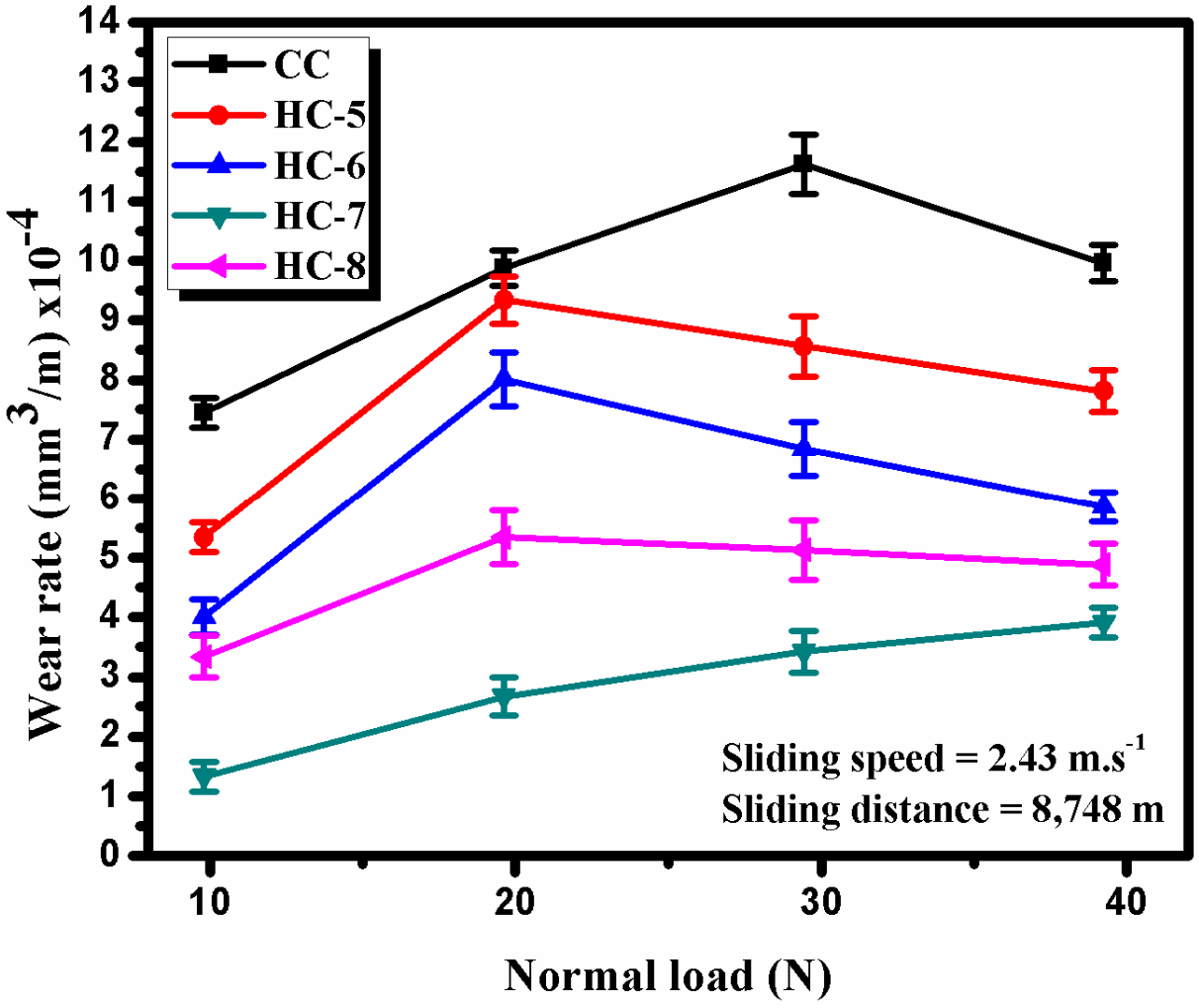

Fig.5.17. Variation of wear rate with normal load at a constant sliding speed of 2.43 $m.s^{-1}$ and sliding distance of 8,748 m

5.3.2.3. Variation of wear coefficient with hardness

The variation of wear coefficient with hardness of CC, HC-5, HC-6, HC-7 and HC-8 at a constant sliding speed of 2.43 $m.s^{-1}$ for the sliding distance of 8,748 m is shown in Fig. 5.18. It can be observed from the Fig.5.18 that the wear coefficient decreases up to HC-7 containing 1.0 wt% B_4C beyond which it increases. CC displays the highest value of wear coefficient however; HC-7 shows the lowest wear coefficient among all the materials investigated in this sturdy as shown in Fig. 5.18.

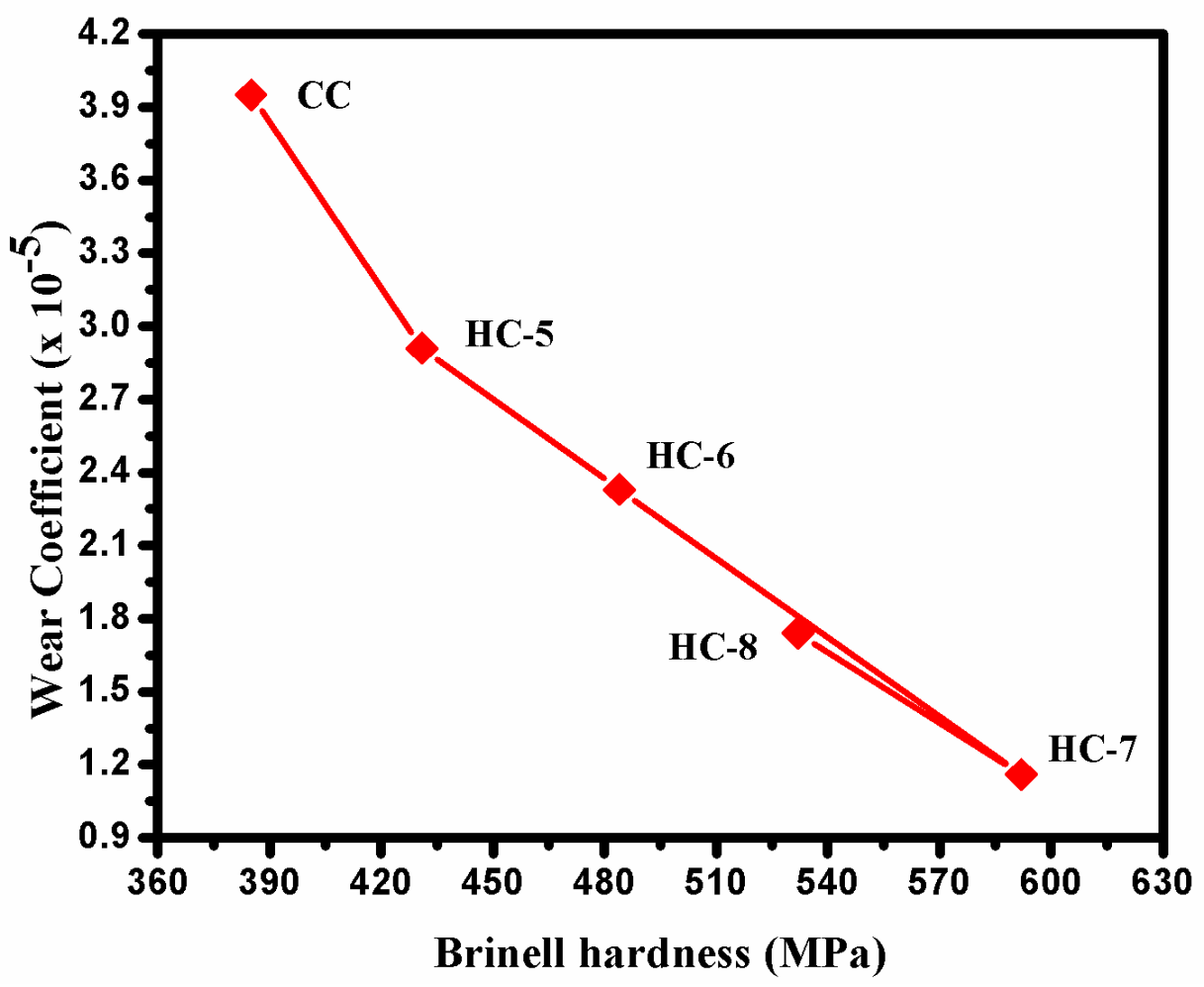

Fig.5.18. Variation of wear coefficient with hardness at a constant sliding speed of 2.43 $m.s^{-1}$ and sliding distance of 8,748 m

5.3.2.4. Variation of wear rate with B_4C content

The effect of B_4C content on the wear rate of HC-5, HC-6, HC-7 and HC-8 at normal loads of 9.81, 19.62, 29.43 and 39.24 N, at constant sliding speed of 2.43 $m.s^{-1}$ for the sliding distance of 8,748 m is shown in Fig. 5.19. It can be observed that the wear rate decreases with increasing B_4C content till 1.0 wt% beyond which it increases at all the applied normal loads. It indicates that the 1.0 wt% of B_4C is the optimum addition under the conditions used in the present study.

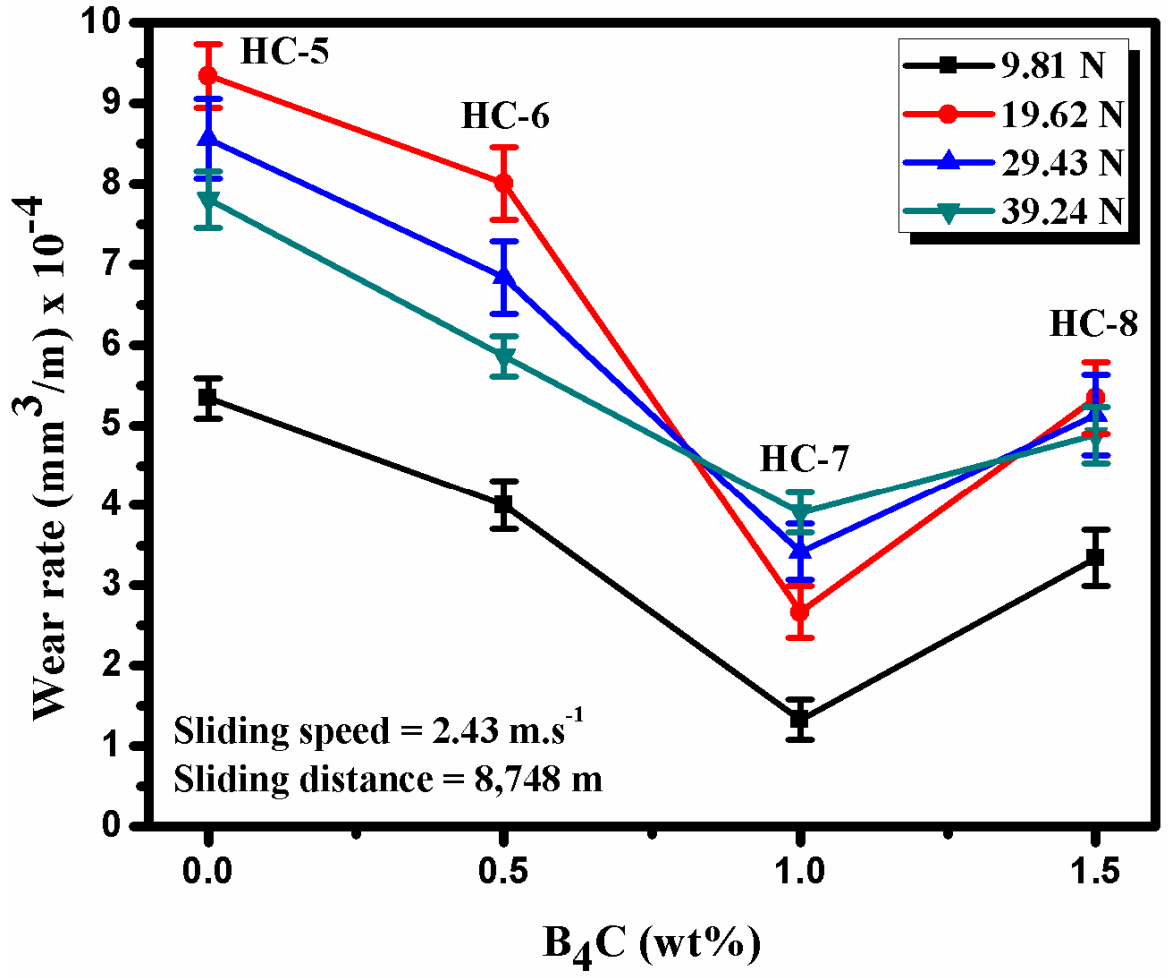

Fig.5.19. Variation of wear rate with B_4C reinforcement at normal load of 9.81, 19.62, 29.43 and 39.24 N for a constant sliding speed of 2.43 $m.s^{-1}$ and sliding distance of 8,748 m

5.3.3. Examination of worn surfaces

5.3.3.1. Worn surfaces at normal load of 9.81 N

Figures 5.20 (a) to (e) show the SEM micrographs of the worn surfaces of CC, HC-5, HC-6, HC-7 and HC-8, respectively, after sliding through a distance of 8,748 m at a normal load of 9.81 N and a constant sliding speed of 2.43 $m.s^{-1}$. Some grooves and delamination running along the direction of sliding could be observed on almost all the worn surfaces of materials investigated. However, the grooves and delamination appear to be deeper in case of CC in comparison to those observed on the worn surface of hybrid composites as evident from Fig. 5.20 (a). The evidence of delamination is not observed on the worn surface of HC-7 as shown in Fig. 5.20 (d). From the Fig. 5.20, it could be observe that the basically two type of wear mechanism i.e. adhesive and abrasive are involved during dry sliding of the materials investigated along with some transfer layers of wear debris. Adhesive wear is dominating over abrasive in CC during dry sliding, however; abrasive and transfer layer of wear debris are mostly observe in the hybrid composites as shown in Figs. 5.20 (a) to (e).

5.3.3.2. Worn surfaces at normal load of 39.24 N

Figures 5.21 (a) to (e) show the typical SEM micrograph of the worn surface of CC, HC-5, HC-6, HC-7 and HC-8, respectively at constant normal load of 39.24 N and sliding speed of 2.43 $m.s^{-1}$ for the sliding distance of 8,748 m. From the Fig. 5.21, it is observed that the morphology of the worn surface of the hybrid composites is significantly different from the worn surface of CC. Severe plastic deformation, delamination, scratch and quit oxidative layers are observed on the worn surfaces of CC as shown in Fig. 5.21 (a). However, quit delamination, abrasion, loose wear debris, oxidative layers along with some transfer layer of

wear debris are observed on the worn surfaces of all hybrid composites as shown in Figs. 5.21 (b) to (e). The worn surfaces of HC-7 and HC-8 display smoother surface compared with others as shown in Figs. 5.21 (d) and (e). Due to some transfer layer of wear debris over the worn surface of HC-7 its worn surface appears very smooth.

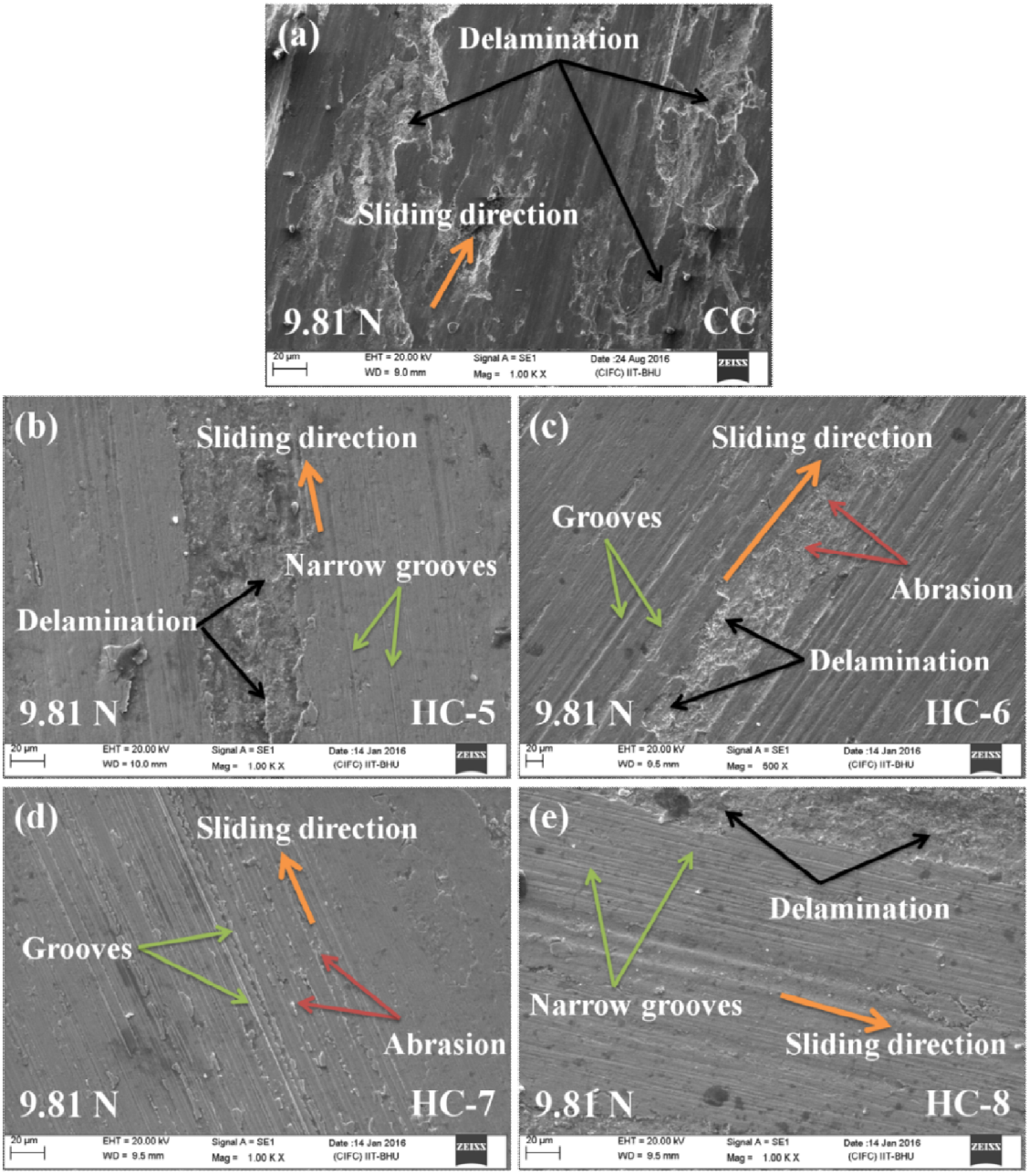

Fig.5.20. SEM micrographs of worn surface of (a) CC, (b) HC-5, (c) HC-6, (d) HC-7 and (e) HC-8 at load of 9.81 N and sliding speed of 2.43 $m.s^{-1}$ for sliding distance of 8,748 m

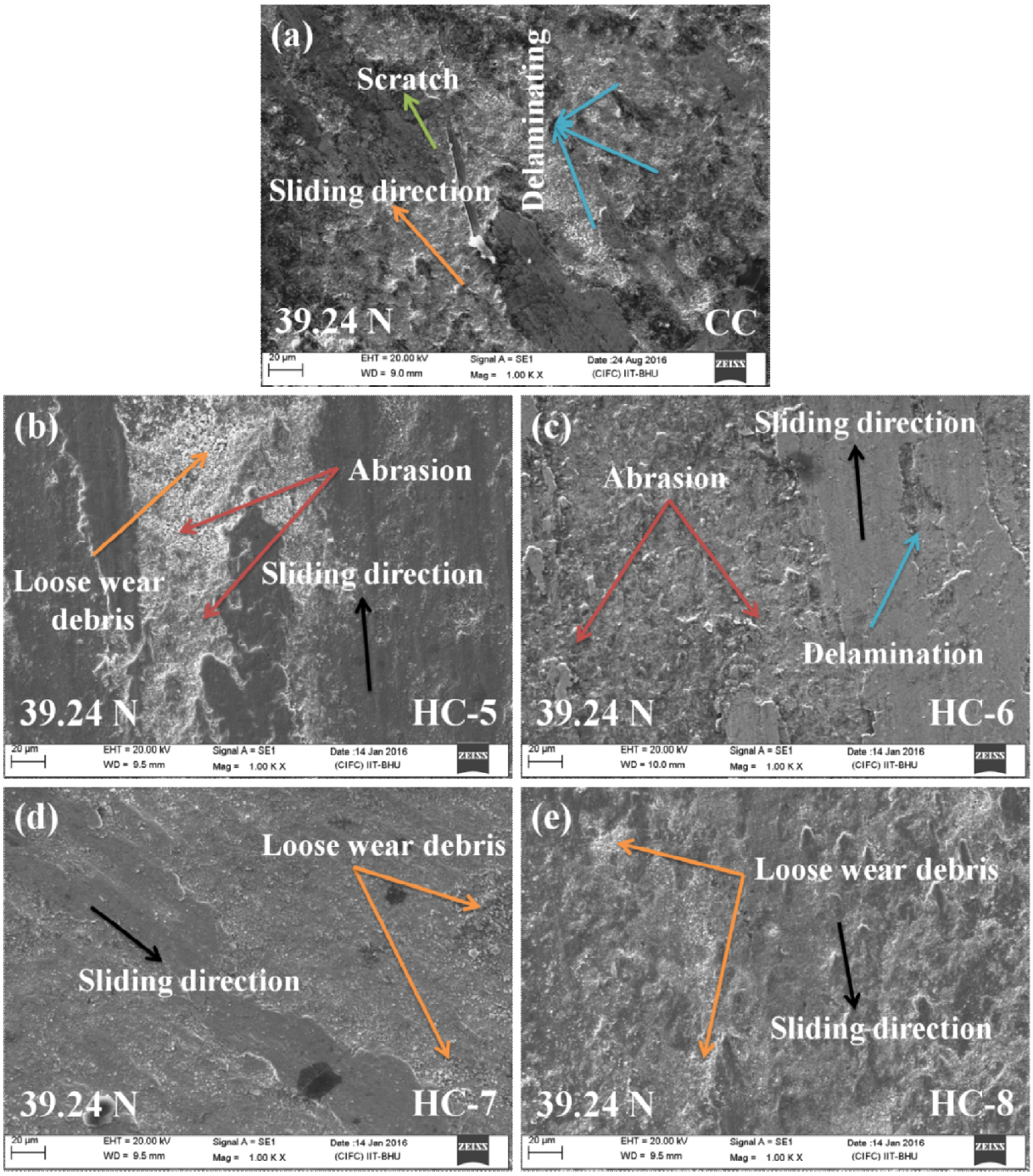

Fig.5.21. SEM micrographs of worn surface of (a) CC, (b) HC-5, (c) HC-6, (d) HC-7 and (e) HC-8 at load of 39.24 N and sliding speed of 2.43 $m.s^{-1}$, for sliding distance of 8,748 m

5.3.3.3. EDAX spectrum of worn surfaces at 39.24 N

The EDAX spectrum of the worn surface of the CC, HC-5, HC-6, HC-7 and HC-8 are shown in Figs. 5.22 (a) to (e), respectively at constant sliding speed of 2.43 $m.s^{-1}$ and normal load of 39.42 N for the sliding distance of 8,748 m. To understand the wear mechanisms which govern the tribological behaviors of CC, HC-5, HC-6, HC-7 and HC-8 during dry sliding this investigation is conducted on worn surfaces of the materials. It is observed that the presence of small intensity peak of the oxygen in the entire EDAX spectrum, its weight and atomic percentage are given in the table just by side their respective spectrums. It indicates that the possible oxide layer has been developed on the worn surfaces of developed materials during the dry sliding. From the Fig. 5.22, it can be observed that the intensity peaks of all the reinforcing elements present in the EDAX spectrum of respective materials except HC-8 in which intensity peak of chromium is missing from the selected area. The EDAX spectrum of worn surfaces of hybrid composites does not display the intensity peak of boron; the reason of absence of boron peak has been explained in detail in Chapter-4. The increase in atomic and weight percentage of carbon intensity peak can be observed in the EDAX spectrum hybrid composites with increasing content of B_4C as shown in Fig. 5.22 (b) to (e).

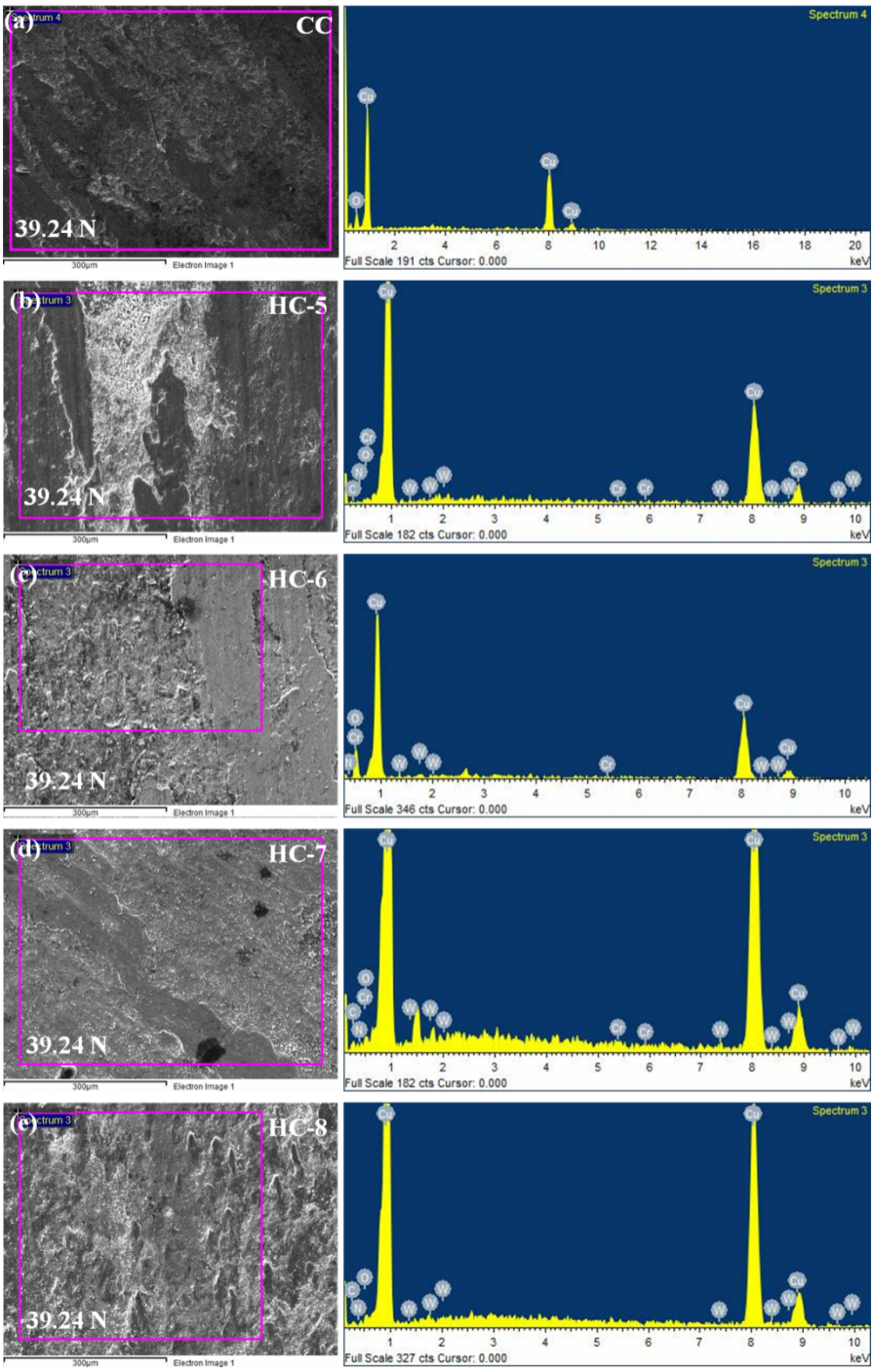

Element	Weight%	Atomic%
O K	10.67	32.18
Cu K	89.33	67.82
Totals	100.00	

Element	Weight%	Atomic%
C K	13.45	39.75
N K	3.40	8.61
O K	3.12	6.93
Cr K	0.04	0.03
Cu K	79.96	44.68
W M	0.03	0.01
Totals	100.00	

Element	Weight%	Atomic%
C K	16.21	36.49
N K	2.11	3.79
O K	17.13	26.92
Cr K	0.29	0.14
Cu K	62.73	32.45
W M	1.53	0.21
Totals	100.00	

Element	Weight%	Atomic%
C K	19.05	48.63
N K	2.31	6.36
O K	2.09	5.03
Cr K	0.41	0.30
Cu K	74.36	39.30
W M	1.77	0.37
Totals	100.00	

Element	Weight%	Atomic%
C K	22.06	56.78
N K	2.28	6.49
O K	1.36	3.39
Cu K	73.59	33.18
W M	0.71	0.16
Totals	100.00	

Fig.5.22. EDAX spectrum of worn surface of (a) CC, (b) HC-5, (c) HC-6, (d) HC-7 and (e) HC-8 at load of 39.24 N and sliding speed of 2.43 $m.s^{-1}$ for sliding distance of 8,748 m

5.3.4. Examination of wear debris

The SEM morphology of the wear debris of CC, HC-5, HC-6, HC-7 and HC-8 are shown in Figs. 5.23 (a) to (e) respectively at sliding speed of 2.43 $m.s^{-1}$ and normal load of 39.24 N after sliding distance of 8,748 m. The morphology of the wear debris of all the materials is studied at same scale of 5000 X. The larger, plate like and flaky geometry of the wear debris of CC are observed as shown in Fig. 5.23 (a). From the Fig. 5.23, it is also observed that the size of wear debris of hybrid composites is comparatively lower than the wear debris of CC. The morphology of the wear debris of hybrid composites displays almost no plate like debris particles as shown in Figs. 5.23 (b) to (e). Some agglomeration can be observed in the morphology of wear debris of HC-5 and HC-6 as shown in Figs. 5.23 (b) to (c) respectively. The morphology of the wear debris of HC-7 displays least debris particles size among all.

5.3.5. AFM analysis of worn surfaces

Figures 5.24 (a) to (e) display the atomic force microscopic (AFM) morphology of the worn surfaces of CC, HC-5, HC-6, HC-7 and HC-8, respectively at constant sliding speed of 2.43 $m.s^{-1}$ and normal load of 39.24 N over the sliding distance of 8,748 m. For quantitative analysis of surface roughness of materials in terms of root-mean-square deviation of profile (R_q) and arithmetical mean deviation of profile (R_a) this characterization is required. From the Figs. 5.24 (a) to (e), it is observed that the R_a and R_q value of worn surface of CC is much higher than the R_a and R_q values of worn surfaces of hybrid composites. Among all the worn surfaces of materials, HC-7 exhibits the least value of R_a (0.012 μm) and R_q (0.018 μm).

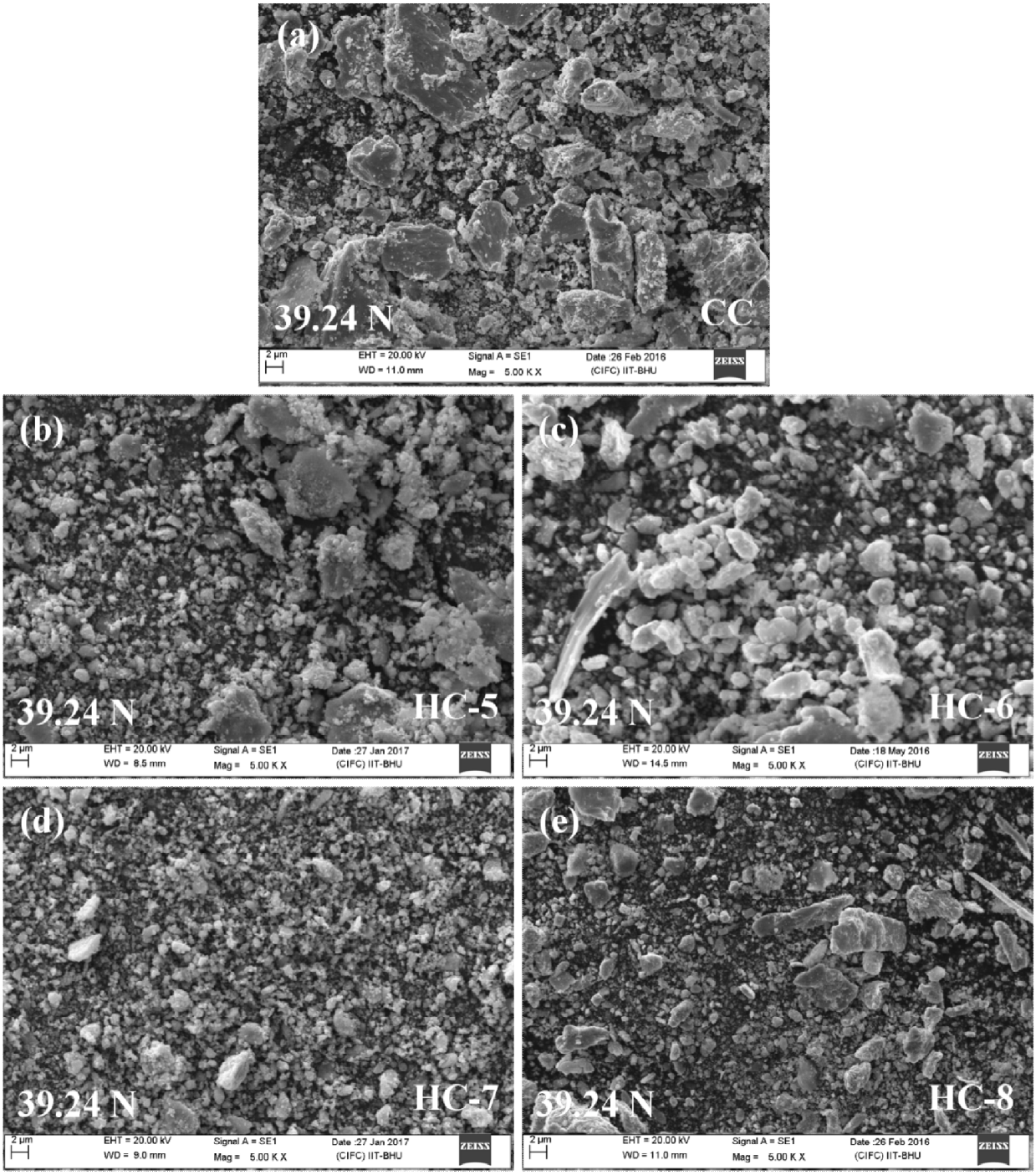

Fig.5.23. SEM morphology of wear debris of (a) CC, (b) HC-5, (c) HC-6, (d) HC-7 and (e) HC-8 at load of 39.24 N and sliding speed of 2.43 $m.s^{-1}$ for sliding distance of 8,748 m

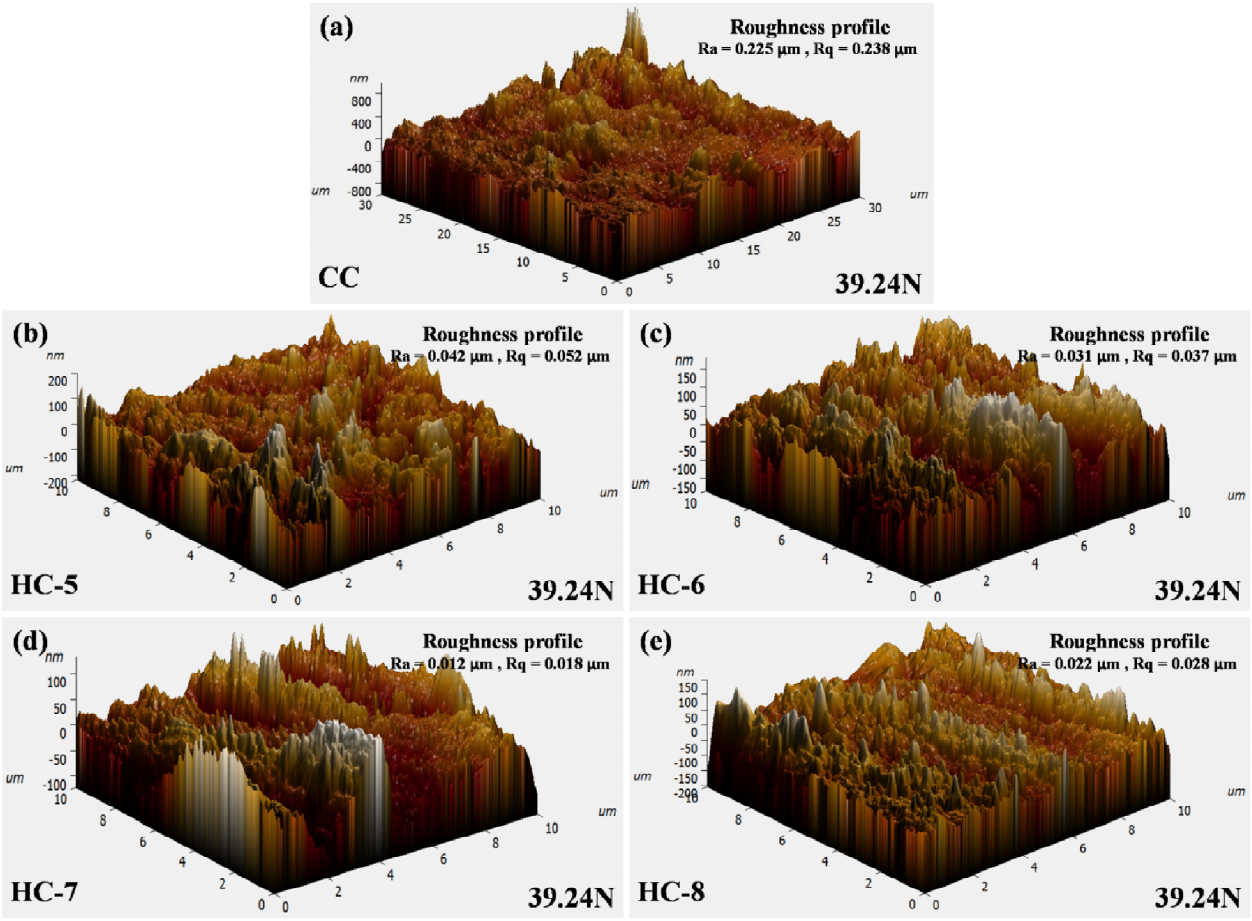

Fig.5.24. AFM morphology of worn surface of (a) CC, (b) HC-5, (c) HC-6, (d) HC-7 and (e) HC-8 at load of 39.24 N and sliding speed of 2.43 $m.s^{-1}$ for sliding distance of 8,748 m

5.4. Comparative study of friction and wear behavior of binary and tertiary reinforced copper-based hybrid composites

Figure 5.25 displays the variation of average friction coefficient with normal load of binary and tertiary reinforced copper hybrid composites at a constant sliding speed of 2.43 $m.s^{-1}$ for sliding distance of 8,748 m. From the Fig. 5.25, it is observed that the average coefficient of friction of binary reinforced hybrid composites (HC-1, HC-2, HC-3 and HC-4) is higher compared with CC, however, the tertiary reinforced hybrid composites (HC-5, HC-6, HC-7 and HC-8) is lower compared with CC at all the applied normal load. The average friction coefficient of both the hybrid composites increases as the normal load increases up to 19.62 N and further it decreases till 39.24 N as depicted in Fig. 5.25. It is also observed that the average coefficient of friction of tertiary reinforced hybrid composites is least among all the materials investigated at the entire applied normal load. The reason behind higher the average coefficient of friction in binary reinforced hybrid composite and lower in tertiary reinforced hybrid composites compared with CC is explained in details in discussion part. Among all investigated materials, HC-4 exhibits the highest average coefficient of friction however; HC-8 shows the lowest average friction coefficient as revealed in Fig. 5.25.

Figure 5.26 shows the behavior of rate of wear with normal load of binary and tertiary reinforced copper hybrid composites at a constant sliding speed of 2.43 $m.s^{-1}$ for sliding distance of 8,748 m. From the Fig. 5.26, it is observed that the rate of wear increases with increase in normal load for all the investigated materials. Both binary and tertiary reinforced hybrid composites reveals lower wear rate compared with CC at all the applied normal load as depicted in Fig. 5.26, the detail explanations of decreasing wear rate is reported in discussion part. However, it is also observed that the wear rate of tertiary reinforced hybrid

composites is lower than binary reinforced hybrid composites at entire applied normal load. The highest and lowest wear rate is observed in CC and HC-7 among all the materials investigated. Therefore, it concludes that the tertiary reinforced hybrid composites are best materials for diverse applications among all the investigated materials in this study.

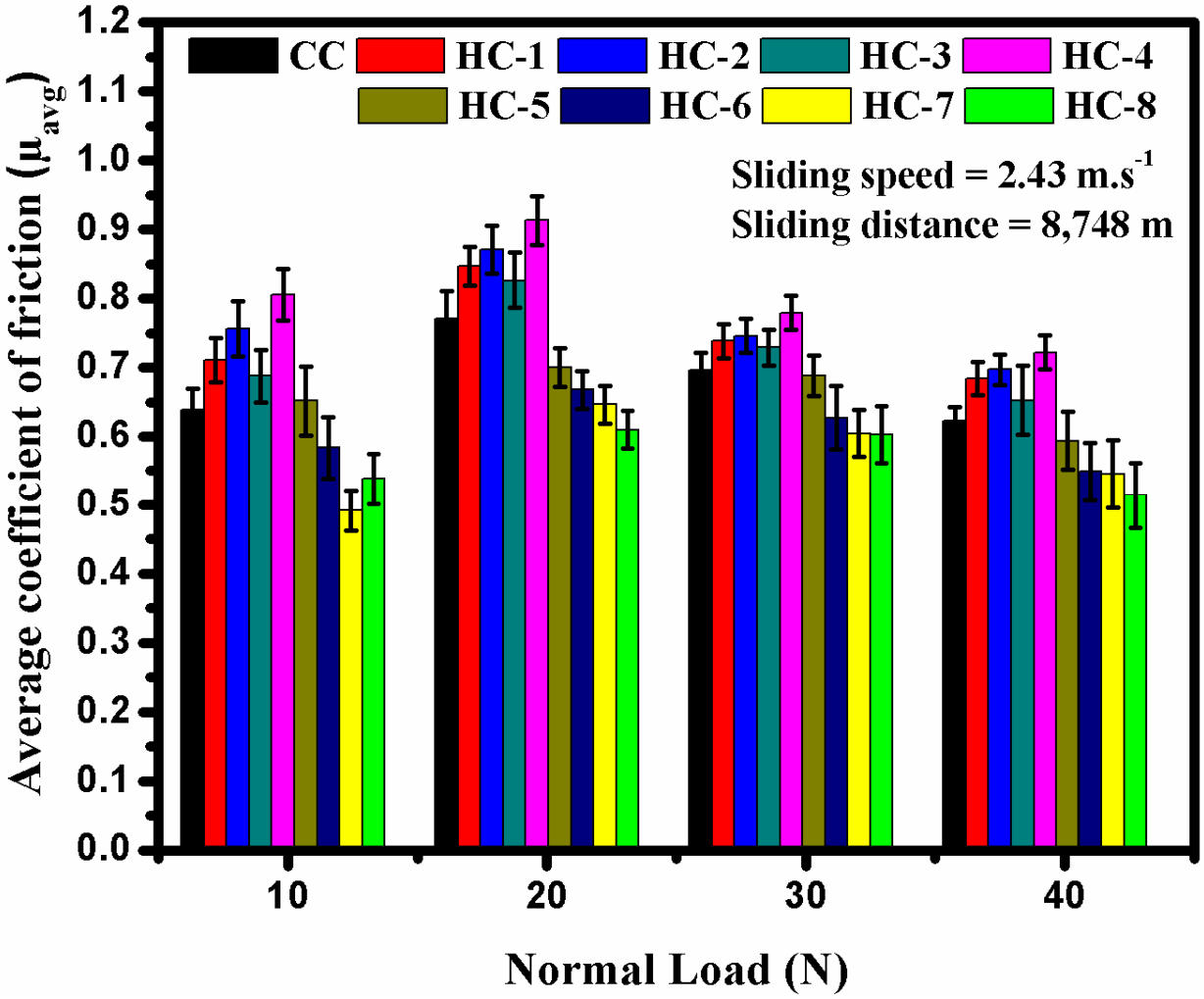

Fig.5.25. Variation of average coefficient of friction with normal load at a constant sliding speed of 2.43 $m.s^{-1}$ and constant sliding distance of 8,748 m

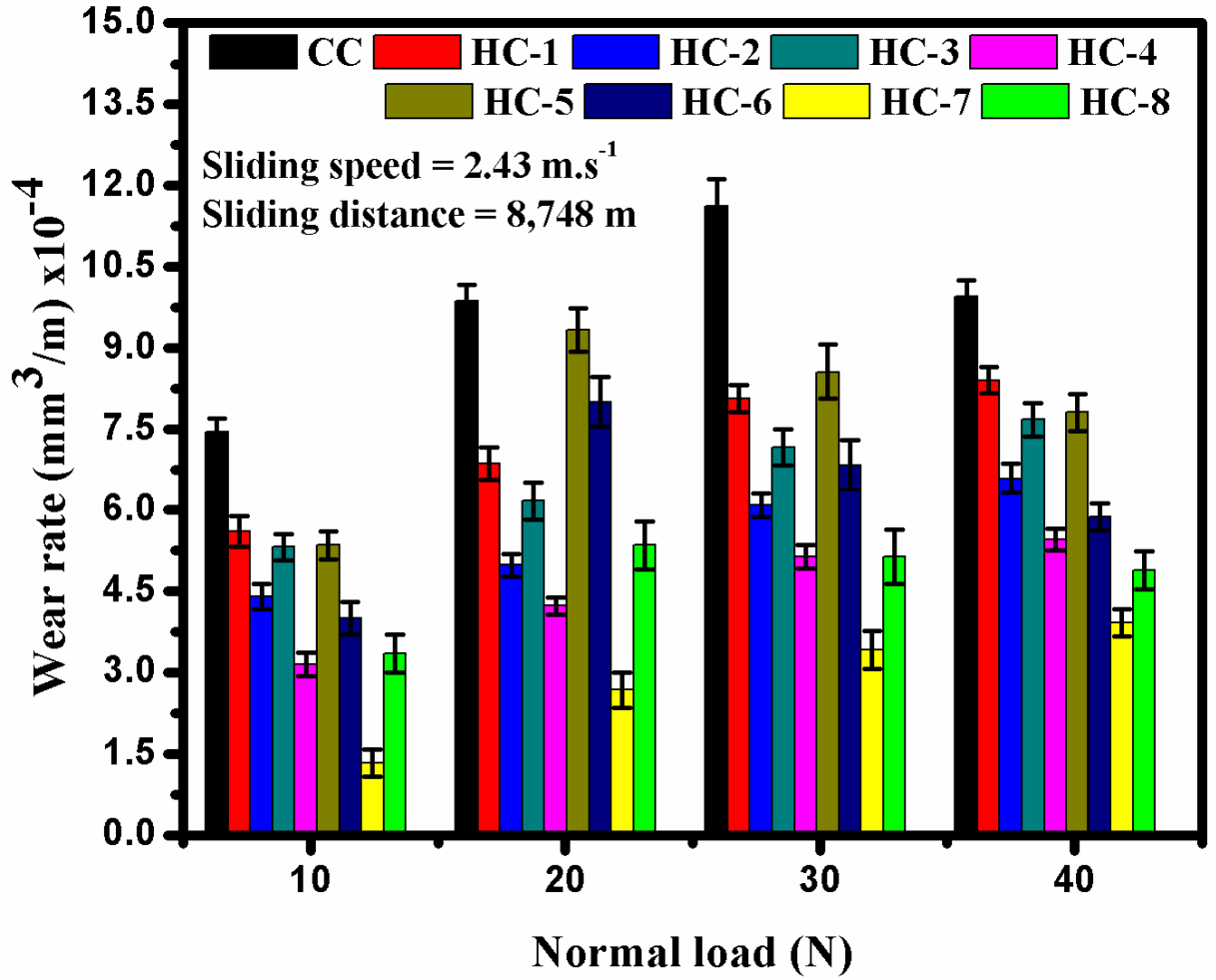

Fig.5.26. Variation of wear rate with normal load at a constant sliding speed of 2.43 $m.s^{-1}$ and sliding distance of 8,748 m

5.5. Discussion

5.5.1. Binary reinforced copper-based hybrid composites

The variation of the friction coefficient with sliding distance of CC, HC-1, HC-2, HC-3 and HC-4 at constant normal loads of 9.81, 19.62, 29.43, 39.24 N and sliding speed of 2.43 $m.s^{-1}$ against the EN31 steel counter face is shown in Figs. 5.1 (a) to (d), respectively. The behavior of friction coefficient with sliding distance is fluctuating in nature, no certain trend is observed. The cause for the fluctuation can be attributed to the disparity in contact that

occurs when the specimen and the counter face are developing a better surface conformity. It has been observed that at low loads such as 9.81 and 19.62 N the fluctuating range varies from 0.4 to 0.97. The least coefficient of friction is observed for CC and most for HC-4. In case of higher loads, the fluctuating range of coefficient of friction is from 0.55 to 0.9 and it can be attributed to the better asperity contact between surfaces of counter disc and wear pin. Overall, CC shows lower friction coefficient than hybrid composite materials.

However, the variation of average friction coefficient with normal load of CC, HC-1, HC-2, HC-3 and HC-4 for sliding distance of 8,748 m at constant sliding speed of 2.43 $m.s^{-1}$ is shown in the Fig. 5.2 respectively. It is found that the average friction coefficient of CC and hybrid composites decreases as the normal load increases. However, it is also observed that the average friction coefficient increases up to normal load of 19.62 N in all the materials investigated. In case of unreinforced copper, increase in average friction coefficient is attributed to the development of oxide layer of copper that is harder than copper. This harder oxide layer offers high coefficient of friction with hard counter face; however as the normal load increases beyond the 19.62 N the developed oxide layer get fractured due to high applied normal load and remove easily from the specimen surface. In addition to this, on application of high normal load that increases the contact area between sample and counter disc surface which may raise the contact temperature and it soften the sample surface. Thus the sample surface tends to slip during high loads there by dropping the average friction coefficient in all case of materials (Rao et al., 2009; Lakshmipathy and Kulendran, 2014). Further, In case of hybrid composites the friction coefficient increases due to the early exposure of the harder ceramic particles and come into contact with the counter surface resulting in increase of friction coefficient due to high abrasion up to normal load of 19.62 N.

However, it decreases beyond normal load of 19.62 N. It can be attributed to the wear debris and pull out reinforced particles from the sample surface which entrap in between the sample and counter surface and may start acting as roller agent that reduces the friction coefficient (Jha et al., 2017). Overall, the average friction coefficient of both CC and hybrid composites decreases on increase in normal load but still the hybrid composite shows a higher value of average friction coefficient compared with CC. Among the hybrid composites, HC-3 has shown the highest average coefficient of friction at all the applied normal loads this may be attributed to the highest hardness shown by this hybrid composite in the present study. This may explain the observed frictional behavior in hybrid composites and it is also evident from Fig. 5.3 which shows the variation of average friction coefficient with hardness of materials used in the present investigation.

Figures 5.4 (a) to (d) show the variation of the cumulative volume loss with sliding distance of materials at constant sliding speed of 2.43 $m.s^{-1}$ and normal loads of 9.81, 19.62, 29.43, and 39.24 N. The cumulative volume loss increases almost linearly with increasing sliding distance in all cases of materials investigated. It can be observed that the volume loss of the CC is consistently higher at all the applied normal loads in comparison to the hybrid composites, which is not surprising because the hard ceramic reinforcement particles provide a shield to the relatively softer matrix during sliding and enhance the load bearing capacity of the hybrid composites leading to a lower loss of materials (Kumar et al., 2014; Nemati et al., 2011). This is attributed to the increase in contact area between wear pin and counter EN31 steel disc due to the combination of different wear mechanism involved. The cumulative volume loss of CC is much higher compared with others because of the temperature of the contacting surfaces increases as the sliding distance increases due to increasing asperity

contacts (Anil et al., 2017). Since, an increase in temperature of the wear pin surface can also be a factor of more volume loss. Due to this increase in temperature the surface of wear pin gets soften which leads to high surface and subsurface damage leading to high volume loss of CC (Rajkumar and Arvindan, 2011). From the Fig. 5, it is observed that the cumulative volume loss with sliding distance of the HC-1, HC-2, HC-3 and HC-4 is comparatively lower than CC, which is attributed to the reinforcement of harder ceramic materials; these hard ceramics particles resist the further wear of the composite materials due to its strengthening effects (Silva et al., 2016). In addition to this, Hassan et al., (2009) also suggested that the role of the reinforcement particles is to support the contact stresses preventing high plastic deformations and abrasion between contacting surfaces and hence to reduce the amount of worn material. Al_2O_3 reinforced copper hybrid composite i.e. HC-2 and HC-4 have low cumulative volume loss with sliding distance compare to others. It is attributed to the high hardness of the materials that obey the Archard's law of wear. Figures 5 (b) to (d) also show the decrease in cumulative volume loss with increasing content of reinforcement from 1 wt to 2 wt% of ZrO_2/Al_2O_3 for the same sliding distance and they follow the almost linear relation with the sliding distance (Kanagaraj et al., 2010).

To understand in more detail regarding wear of materials during sliding the behavior of wear rate with normal load is analyzed. Figure 5.5 shows the variation of the wear rate with normal load of materials at constant sliding speed of 2.43 $m.s^{-1}$ and for sliding distance of 8,748 m. It is observed that the wear rate increases as the normal load increases from 9.81 to 39.24 N for all materials investigated (Walid et al., 2009; Zhan and Zhou, 2005; Zhan et al., 2004). The extent of plastic deformation is high at higher normal loads which promotes higher wear rates in all samples. It can be seen from Fig. 5.5 that the wear rate increases

almost linearly with the load following Archard's law which states that wear rate is directly proportional to the normal load but inversely proportional to the hardness of the softer of the two mating materials (Archard, 1953). It can be expressed mathematically as,

$$w = k\frac{LS}{H} \qquad (5.1)$$

where, W is wear volume loss, K is the wear coefficient, L is the applied load, S is the sliding distance and H is the hardness of softer material. However, the hybrid composites have a lower wear rate than the CC at all the loads, which may be attributed to the higher hardness of the composites in comparison to the CC. The increasing rate of wear with normal load may be explained on the basis of the generation of more debris at relatively higher load leading to a higher loss of material and thus, the wear rate. In case of CC, it can be presumed that there is a possibility of direct metal-metal contact and this phenomenon may promote the adhesive wear mechanism and consequently the plastic deformation takes place and the wear rate of matrix increases as compared to the hybrid composite specimens. The CC shows the fastest increase in wear rate as compared with hybrid composites. In addition to this, there are possible reasons for high wear rate in pure copper first, due to its lower micro hardness compared with hybrid composites that lead to high wear rate which is motivated by the delamination phenomenon. Second, high wear rate in CC can be attributed to the formation of oxide layer when the temperature increases due to high friction at higher normal load, and the developed oxide layer gets fractured and remove the materials in greater extent, it can be observed in the Fig. 5.9 (a). Therefore, a comparison of Figs. 5.7 (a) and 5.8 (a) which correspond to the worn surface of CC at loads of 9.8 and 39.24 N, respectively, shows that CC has deeper grooves along with signs of plastic deformation with increasing loads. Whereas, in case hybrid composites the wear rate increases as the load increases that is

attributed to the load effect on the wear pin i.e. the depth of penetration of the harder ceramic reinforcements in the soft matrix increases as the normal load increases, and it is also motivated by increase in the temperature of the pin surface. The increase in temperature makes the matrix surface more ductile so penetrations are highly envisaged. Therefore, harder ceramic like- WC, Al_2O_3 and ZrO_2 push back into the matrix and starts wear of matrix materials in form of plastic deformation of sub surfaces by the hard counter disc surface. However, it is observed that the hybrid composites have low wear rate compared with CC, this is attributed to the improved hardness of the hybrid composites due to the harder ceramics addition, which follows the Archard's law of wear (Tjong and Lau, 2000; Tjong and Lau, 2000). The behavior of wear rate with hardness can be seen in the Fig. 5.6 which complying the results reported above. In addition to this, the harder ceramic reinforcements render remarkable resistance to plastic deformation and reduce the adhesion between the hybrid composites pin and counter steel disc. Apart from this, the ceramic reinforcements act as load bearing components in the hybrid composites which significantly reduces the contact area between copper matrix and counter steel disc. Therefore, with the reduced contact area, the deterioration of pin is less (Mallikarjuna et al., 2017). In support of this, low wear in all the hybrid composites may also be attributed to the possible transfer layer which is helpful in protecting the underlying material against wear that can be seen in Figs. 5.9 (b) to (d).

During dry sliding of materials which kind of wear mechanism involved therefore the morphological study of worn surfaces is done at constant normal load of 9.81 and 39.24 N, sliding speed of 2.43 $m.s^{-1}$ for the sliding distance of 8,748 m which is shown in Figs. 5.7 and 5.8, respectively. In contrast, the morphology of the worn surface of the hybrid composites is significantly different from the worn surface of CC at both the normal loads. The severe

plastic deformation and ploughing in worn surface of CC are observed as the load increases from 9.81 to 39.24 N as shown in Fig. 5.8 (a). The formation of grooves on the worn surface of CC may be attributed to formation of copper oxide, which is confirmed by EDAX investigation on worn surface of CC as shown in Fig. 9 (a). During the dry sliding test, the temperature rise due to frictional heating between pin and counter disc may led to reaction between copper and atmospheric oxygen developing its oxides. The developed copper oxides are hard in nature get embedded in the debris and account for ploughing of pin surface in the form of grooves (Mallikarjuna et al., 2017). It is observed that the morphology of worn surface of hybrid composites is smoother as compared with worn surface of CC at both the normal load. It is attributed to the harder ceramics reinforcement which improves the wear resistance against dry sliding by restricting the deformation of the copper matrix. It is due to the improved hardness of hybrid composites results in significant reduction in the localized plastic deformation of the pin surfaces (Rajkumar and Arvindan, 2011) that can be observed in the SEM micrographs of worn surface hybrid composites. It is also supported by the transfer of layer that can be observe in the EDAX analysis of worn surfaces of hybrid composites as shown in Figs. 5.9 (b) to (e). The delamination, mechanical mixed layer (MML), narrow grooves, wear debris and micro cracks are observed in the worn surfaces of the materials, due to different wear mechanism involved during dry sliding as shown in Fig. 5.8 at higher normal load. The grooves are found on the worn surfaces that are attributed to the ploughing through hard asperities of counter steel surface or ploughing through detached harder ceramic particles from pin surface (Li et al., 2015).

Figures 5.9 (a) to (f) show the EDAX spectrum of the worn surface of CC, HC-1, HC-2, HC-3 and HC-4. It is observed that the presence of small intensity peak of the oxygen

in the entire EDAX spectrum, its weight and atomic percentage are given in the table just side by the spectrums. It indicates that the oxide layer has been developed on the worn surfaces of developed materials during the dry sliding. It may be attributed to the increase in the temperature of the surfaces during sliding against the hard steel counter surface; such increase in temperature is prone to oxidation (Rajkumar and Arvindan, 2011). The small intensity peak of iron is also observed in all the EDAX spectrum of composite and hybrid composites, their weight and atomic percentage are reported in the table. It can be attributed to the harder ceramic reinforcements in composite and hybrid composites, which abrade some amount of materials from the hard steel counter surface after long sliding distance and get stick or transfer with the pin surface of hybrid composites. The presence of iron and oxygen intensity peak in the spectrum also indicates that the mechanically mixed layer has been developed on the worn surface of the materials (Janbozorgi et al., 2017). Therefore, the investigation of worn surface of all materials suggest the wear mechanism involved in pure copper is quite seizing and oxidative wear proceeded by the delamination of subsurface layers develop the severe worn surface. However, the oxidative and abrasive wear is mainly involved in case of hybrid composites without any seizing wear.

After various characterizations, it has been observed that the hybrid composite exhibits better tribological behavior compared with CC. It is further justified with the analysis of wear debris and worn surfaces through SEM and AFM of CC, HC-1, HC-2, HC-3 and HC-4 at 39.24 N and sliding speed of 2.43 $m.s^{-1}$ as shown in Figs. 5.10 (a) to (e) and 5.11 (a) to (e) respectively. From the Figs. 5.10 (a) to (e), it is observed that the debris particles of hybrid composites are smaller and equiaxed compared with CC. it is attributed to the high hardness of the hybrid composites. However, the wear debris of CC is larger, flaky and plate

like morphology due the severe plastic deformation and adhesive wear involvement mainly as shown in Fig. 5.10 (a). Whereas, the wear debris of HC-4 shows the smallest wear debris among all. As shown in Fig. 5.10 (e). From the Figs. 5.11 (a) to (e), it is observed that the R_a and R_q of hybrid composites are much lower compared with CC due to its low volume loss. So, these investigations also added confirmation the above explanation regarding low wear of hybrid composites compared with CC under the same conditions of loads, sliding speed and sliding distance.

5.5.2. Tertiary reinforced copper-based hybrid composites

Figures 5.12 (a) to (d) show the variation of coefficient of friction with sliding distance at normal load of 9.81, 19.62, 29.43 and 39.24 N for CC, HC-5, HC-6, HC-7 and HC-8 at a constant sliding speed of 2.43 $m.s^{-1}$ against the EN31 steel counter face, respectively. From Figs. 5.12 (a) to (d), fluctuating nature of coefficient of friction without a certain trend is observed with respect to sliding distance at all the applied normal loads. It may be attributed to the disparity in contact that occurs when the specimen and the counter face are evolving to develop a better surface conformity similar to case of binary reinforced hybrid composites.

However to explore more the behavior of coefficient of friction of tertiary reinforced hybrid composites, average coefficient of friction with respect to normal load and content of B_4C are studied. Figs. 5.13 and 5.15 display the variations of average coefficient of friction with normal load and B_4C content at a constant sliding speed of 2.43 $m.s^{-1}$ for sliding distance of 8,748 m for CC, HC-5, HC-6, HC-7 and HC-8, respectively. From both the Fig. 5.13 and Fig. 5.15, it is observed that the average friction coefficient decreases with

increasing both the normal load and the amount of B_4C. The average friction coefficient decreases with the increasing B_4C content in the tertiary hybrid composites at all the normal load as evident from Fig. 5.15. It may be attributed to the following two reasons (i) reinforcing B_4C, BN and WC particles that are detached from the matrix and get trapped between the contacting surfaces start acting the rolling particles which reduces the metal to metal contact and (ii) due to quit lubricating nature of BN and B_4C particles which allow to slide the two mating surfaces to each other easily, their presence can be observed in the respective EDAX spectrum as shown in Fig. 5.22. At relatively higher loads, more these reinforcing particles are expected to get detached and squeeze out from the softer matrix surface with increasing load which may further promote the similar phenomenon which has discussed above resulting in an decrease in average friction coefficient in the tertiary reinforced hybrid composites. An increase in the B_4C content further aggravates the situation as more number of particles now gets detached and will promote the similar action in greater extent as discussed above. Therefore, the average friction coefficient decreased with increase in both the normal load and the B_4C content. However, the variation of average coefficient of friction of CC with respect to normal load has been discussed above as in binary reinforced hybrid composites.

The variation of cumulative volume loss with respect to sliding distance for CC, HC-5, HC-6, HC-7 and HC-8 under different loads of 9.81, 19.62, 29.43, 39.24 N and at a constant sliding speed of 2.43 $m.s^{-1}$ as shown in Figs. 5.16 (a) to (d), respectively. From the Figs. 5.16 (a) to (d), it is observed that the cumulative volume loss increases with increasing sliding distance almost linearly. It is also observed that the cumulative volume loss of the CC is consistently higher at all the applied normal loads in comparison to the tertiary reinforced

hybrid composites. The lower cumulative volume loss in tertiary hybrid composites is attributed to the hard ceramic reinforcing particles such as B_4C, BN and WC provide a shield to the relatively softer copper matrix during dry sliding and improve the load bearing capacity of the tertiary hybrid composites leading to a lower volume loss of material (Kumar et al., 2014; Nemati et al., 2011). The importance of the reinforcement particles is to withstand the contact stresses preventing high plastic deformations and abrasion between mating surfaces, similar phenomenon is also suggested by Hassan et al., (2009). Among the tertiary hybrid composites, HC-7 has shown the lowest cumulative volume loss consistently at all the normal loads, followed by HC-8, HC-6 and HC-5 in increasing order. This may be explained on the basis of the hardness of the tertiary hybrid composites. Since, the hardness of HC-7 is the highest and it is lowest in HC-5 among tertiary hybrid composites in the present investigation.

Figure 5.17 displays the variation of the wear rate of the CC, HC-5, HC-6, HC-7 and HC-8 with respect to normal load at constant sliding speed of 2.43 $m.s^{-1}$, for sliding distance of 8,748 m. From Fig. 5.17, it is observed that the wear rate increases almost linearly with the applied normal load following Archard's law which defines that wear rate is directly proportional to the normal load but inversely proportional to the hardness of the softer of the two mating materials (Archard, 1953). However, the tertiary hybrid composites have a lower wear rate than the CC at all the loads, which may be attributed to the higher hardness of the tertiary hybrid composites as compared to the CC. It can be understand in more detail by the plot between wear coefficients and hardness where, the wear coefficient decreases with increasing hardness of the materials as shown in Fig. 5.18. The increasing rate of wear with normal load may be explained on the basis of the generation of more wear debris and

detachment of harder particles at relatively higher load leading to a higher loss of material and thus, the wear rate. In case of CC, it can be presumed that there is a possibility of direct metal-metal contact and this phenomenon may promote the adhesive wear mechanism and consequently the plastic deformation takes place and the wear rate of CC increases as compared to the tertiary hybrid composite specimens.

The effect of weight percentage of B_4C particles with constant weight percentage of BN and WC on the wear rate of tertiary reinforced copper hybrid composites is shown in Fig. 5.19. The wear rate decreases when the weight percentage of B_4C is increases up to 1.0 wt% and further it decreases. The wear rate is found to be 9.4×10^{-4} mm^3/m at 0 wt% and 3.1×10^{-4} mm^3/m at 1.0 wt% with constant wt% of BN and WC at 19.62 N. It is obvious that the improvement in hardness of the hybrid composites would lead to enhancement of wear resistance that follow the Archard's law. The enhancement in wear resistance of tertiary reinforced hybrid composites may be attributed to the following factors; (i) B_4C particles including with BN and WC refine the crystal grains of copper; (ii) the dispersion of B_4C particles including with BN and WC all over the copper metal matrix which can provide Orowan strengthening (Zhang et al, 2008); (iii) good interfacial bonding between B_4C, BN and WC particles and copper matrix which delays the detachment of particles during dry sliding action and (iv) Since, B_4C and BN particles well known as solid lubricants so may offer some lubricating action during the dry sliding. The effect of these factors increases when the weight percentage of B_4C particles increases due to the higher volume fraction of B_4C particles; it further enhances the wear resistance of the tertiary reinforced copper hybrid composites.

The worn surfaces of the CC and tertiary reinforced hybrid composites with variable wt% of B_4C at 9.81, 39.24 N are shown in the Figs. 5.20 (a) to (e) and 5.21 (a) to (e), respectively. But the morphology of worn surface at low load does not reveal the exact wear mechanism, however it is observed clearly at higher load. From the Figs. 5.21 (a) to (e), it is observed that there is a significant difference in the morphology of the worn surfaces. The degree of subsurface deformation decreases and the plowing marks and scratch disappear on the worn surface when weight percentage of B_4C is increased. The worn surface of CC shows severe plastic deformation and material removal as shown in Fig. 5.21 (a). Where, the copper is directly exposed to the cutting action of the counter face material in the absence of any kind of reinforcing particles which causes high rate of material removal. When, the weight percentage of B_4C particles increases with constant weight percentage of BN and WC, the increased content of B_4C particles helps the copper matrix to offer resistance to the cutting action as well as restrict the plastic deformation during dry sliding action. Hence, the rate of metal removal decreases as weight percentage of B_4C is increased. When the volume fraction of B_4C particles is 1.0 and 1.5 wt%, the worn surface is observed to be uniform due to higher content of B_4C particles as shown in Figs. 5.21 (d) and (e). It is observed that the worn surface is almost covered with debris, no apparent cracks or subsurface deformation. The debris does not adhere to the worn surface due to the hard nature of the B_4C particles including BN and WC, loose wear debris can be observe in Figs. 5.21 (b) to (e). When, the weight percentage of B_4C particles is increased, the wear mode changes from adhesive and micro cutting as shown in Fig. 5.21 (a) to abrasive as shown in Figs. 5.21 (d) and (e) (Sathiskumar et al., 2013).

The effect of weight percentage of B_4C particles on the wear debris of CC and tertiary reinforced hybrid composites at 39.24 N is shown in Figs. 5.23 (a) to (e). There is a significant change in the size of the wear debris observed. The size of wear debris is large for CC and HC-5 with 0 wt% of B_4C particles as compared to others as shown in Figs. 5.23 (a) and (b). The large size of wear debris can be attributed to the more adhesion and micro cutting action of the counter face. When, the weight percentage of B_4C increases beyond 0 wt%, the size of wear debris decreases considerably. The size of wear debris is very fine when the weight percentage of B_4C is 1.0 as shown in Fig. 5.23 (d). The formation of fine wear debris can be attributed to the following three factors: (i) increased hardness of the hybrid composites, (ii) possible lubricating action provided by the B_4C and BN particles and (iii) decreased probability of direct contact between wear specimen and counter face due to the presence of B_4C, BN and WC particles. However, the detached B_4C, BN and WC particles during sliding may convert two body abrasion wear to three body abrasion wear which results in the generation of fine debris also (Sathiskumar et al., 2013). The worn surface analysis using SEM reveals the loose wear debris and abrasive action as shown Figs. 5.21 (b) to (e), however EDAX spectrum of worn surfaces display the presence of intensity peak of boron, nitride, oxide and carbide as shown in Figs. 5.22 (b) to (e) which support its wear mechanisms and reason for fine wear debris.

In comparative study of the dry slinging friction and wear behavior of binary and tertiary reinforced hybrid composites. It is observed that the coefficient of friction of tertiary hybrid composites is lower than binary reinforced hybrid composites at all the applied normal load of 9.81, 19.62, 29.43 and 39.24 N as shown in Fig. 5.25. It may be attributing to the higher hardness of the tertiary hybrid composites which develop less real asperity contact

with asperity of the counter surfaces. In addition to this, the reinforcement phase in tertiary hybrid composites act as solid lubricants between the surfaces of pin and disc when it comes out from the matrix phases during dry sliding. The wear rate of the tertiary hybrid composites is also found lower compared with binary hybrid composites at all the applied normal load as shown in Fig. 5.26. This low wear rate in tertiary hybrid composites is attributed to it's the higher hardness compared with binary hybrid composites which follow the Archard's law of wear which suggest that the wear rate is inversely proportional to the hardness of the softer materials. The low wear may also be attributed to its low coefficient of friction.